Nonlinear Mixed Finite Element Analysis for Contact Problems by a Penalty Constraint Technique

by

Ganesh R. Kalpundi

Thesis submitted to the Faculty of the

Virginia Polytechnic Institute and State University

in partial fulfillment of the requirements for the degree of

Master of Science

in

Engineering Mechanics

APPROVED:

Dr. Surot Thangjitham, Chairman

Dr. Robert A. Heller

Dr. Rakesh K. Kapania

August, 1993

Blacksburg, Virginia

Nonlinear Mixed Finite Element Analysis for Contact Problems by a Penalty Constraint Technique

by

Ganesh R. Kalpundi

Dr. Surot Thangjitham, Chairman

Engineering Mechanics

(ABSTRACT)

A nonlinear mixed finite element formulation based on the Hellinger-Reissner variational principle is developed for planar contact stress analysis. The formulation is based on the updated Lagrangian approach and accounts for geometric nonlinearity. In the mixed model, both displacements and stresses are approximated independently and this approach has in general been found to be more accurate than the displacement finite element model, especially for contact problems since it avoids the extrapolation of stresses computed at the Gauss points to the boundary nodes.

An algorithm based on the penalty technique for equality constraints has been developed to handle the interface boundary conditions arising in a contact problem. The algorithm automatically tracks potential contact nodes, detects overlap during any load step and iteratively restores geometric compatibility at the contact surface. The classical Hertz contact problem is solved to validate the algorithm.

The mixed formulation algorithm in cylindrical coordinates is applied in conjunction with the penalty based algorithm to solve the contact problem in layered cylindrical bodies. Static condensation techniques are used to condense out the discontinuous components of stresses at the element level. The contact stress distribution and variation of contact area with load is computed for different loading situations. Furthermore, the effect of the difference in the rela-

tive magnitudes of the moduli of the layers on the stability of the contact algorithm is investigated.

Acknowledgements

I am very thankful to my advisor, Dr. Surot Thangjitham for his continuous support and guidance. His encouragement was instrumental in the successful completion of this work.

My sincere thanks to Drs. Robert Heller and Rakesh Kapania for serving on my graduate committee and for their valuable suggestions. Their recommendations greatly improved this work.

I am also grateful to Dr. J.N. Reddy for his invaluable guidance during the initial stages of this work.

I am greatly indebted to my parents, Ramamurthy and Krishnakumari for their constant encouragement and love throughout my education.

Finally, I would like to convey my thanks and appreciation to my friends here at Virginia Tech who helped me in numerous ways. I would especially like to thank Dr. I. Janajreh, Dr. X. Wang, Dr. Y.S. Reddy, J. Pandrangi and N. Vure.

Table of Contents

List of Illustrations

List of Tables

Chapter I

INTRODUCTION

1.1 The contact problem

The evaluation of the stresses and deformation when two or more solid bodies are brought into contact as a result of external loading constitutes a contact problem. When the type of contact is non-conforming (i.e. the bodies coming into contact have dissimilar profiles), the area of contact is much smaller compared to the dimensions of the bodies themselves. As a result the stresses are highly concentrated in the region of contact and are independent of the distribution of stresses in the bulk of the bodies. Hence the contact stresses constitute a local stress concentration that can be significantly high and can lead to failure of the structure. Thus in a contact problem one is interested in the stresses in the vicinity of the contact region as opposed to other problems wherein the region of interest is far removed from the point of application of load.

There are other significant differences that set apart the contact problem from other problems of linear elasticity. The foremost characteristic is that prior to the application of loads to the

body, the extent of the contact surface (area on which the contacting bodies meet) is not known. As a result, the boundary conditions on this contact surface (stresses and displacements) are also unknown. Hence, even if one were to neglect the imminent finite strains and material non-linearities, the progressive change of contact surface in itself presents a kind of surface non-linearity. In addition, the surface of contact may be frictional or frictionless and appropriate slip criteria need to be adopted to accurately model the particular case. Thus the contact problem is inherently non-linear.

1.2 Solution of contact problems

Historically, the study of contact problems was motivated by attempts to put forth acceptable theories of impact of colliding bodies[1]. In 1882, Heinrich Hertz solved the static contact problem in elasticity[2]. This marked the advent of the subject of contact mechanics. Although exact, the Hertz theory is restricted to idealizations like perfectly elastic solids, small strains, frictionless surfaces and specific geometric configurations. Some of the other authors who presented exact solutions to specific problems are Muskhelishvili[3], Gladwell[4] and Johnson[5].

Exact solutions using the classical approach are not possible or are very difficult to obtain when dealing with arbitrary geometrical configurations and/or nonhomogenous materials. Typically, the contact problem is idealized by introducing concentrated forces, support conditions or some form of pressure distribution. However, such approximations are not true representations of the interface conditions that characterize a contact problem. This has necessitated the use of numerical techniques like the finite element method which has the inherent capability to handle problems with varying geometry, material and loading conditions and can also provide realistic solutions.

Different methods are available for solving the contact problem using the finite element method. These range from special interface elements to surface algorithms. A popular element used widely in commercial codes for handling contact problems is the gap element [6] [7]. Gap elements are used to connect two or more bodies which may come into contact as a result of loading. Gap elements usually consist of a truss element with bilinear material properties. Two surfaces connected by gap elements are shown in Fig.[1.1]. Since truss elements are one dimensional they provide stiffness against motion normal to the line of contact. If the bodies come into contact, a compressive force must exist at the interface and if they lose contact, the force should be tensile or close to zero. To account for this behaviour, the gap element should exhibit bilinear stiffness as shown in Fig.[1.2]. As can be seen, the element has a high stiffness in compression and a very low stiffness in tension. Another element that is used in contact problems is the area interface element shown in Fig. [1.3]. These elements also use material properties similar to the gap elements to account for the separation and closing. A major disadvantage in using gap or interface elements is that they require matching nodes and spacing along the potential contact surfaces. An alternative to using such elements is the surface algorithm approach wherein the algorithm continually checks for penetration of one component by the boundary of the other and then pushes it back. These algorithms do not suffer from the disadvantage that gap elements or interface elements do, that is, thay do not require the meshing to be done in any particular fashion on the contacting surfaces. In the present work also such an algorithm has been developed.

1.3 Mixed elements vs standard elements for contact analysis

The displacement finite element method based on the minimization of the total potential energy is well established and a vast amount of literature describing the method can be found [8],[9]. Hence most of the literature dealing with the solution of contact problems is based on this method. However, the mixed finite element method is gaining popularity in the analysis

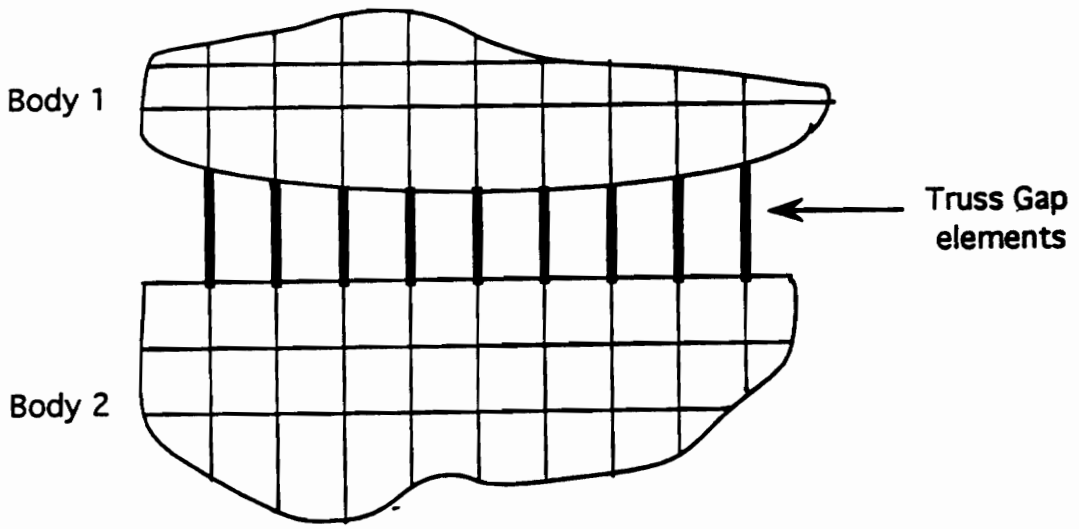

Figure 1.1. Two surfaces connected by gap elements

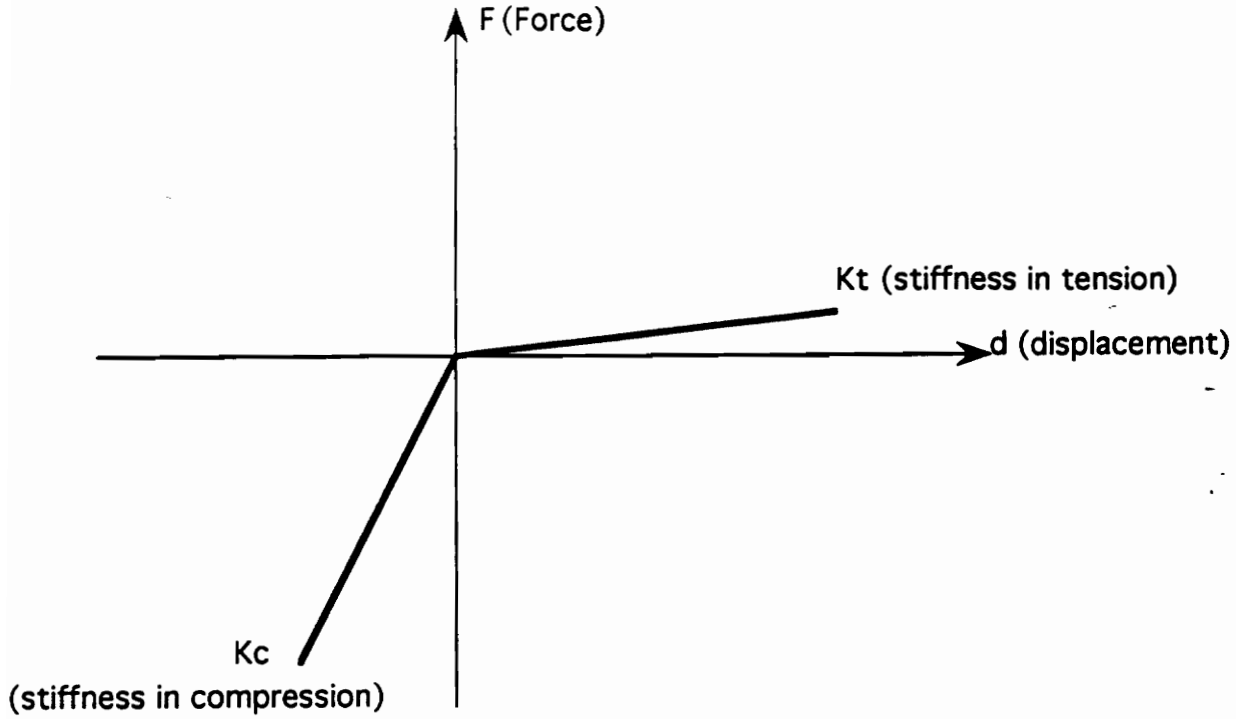

Figure 1.2. Bilinear normal stiffness of gap elements

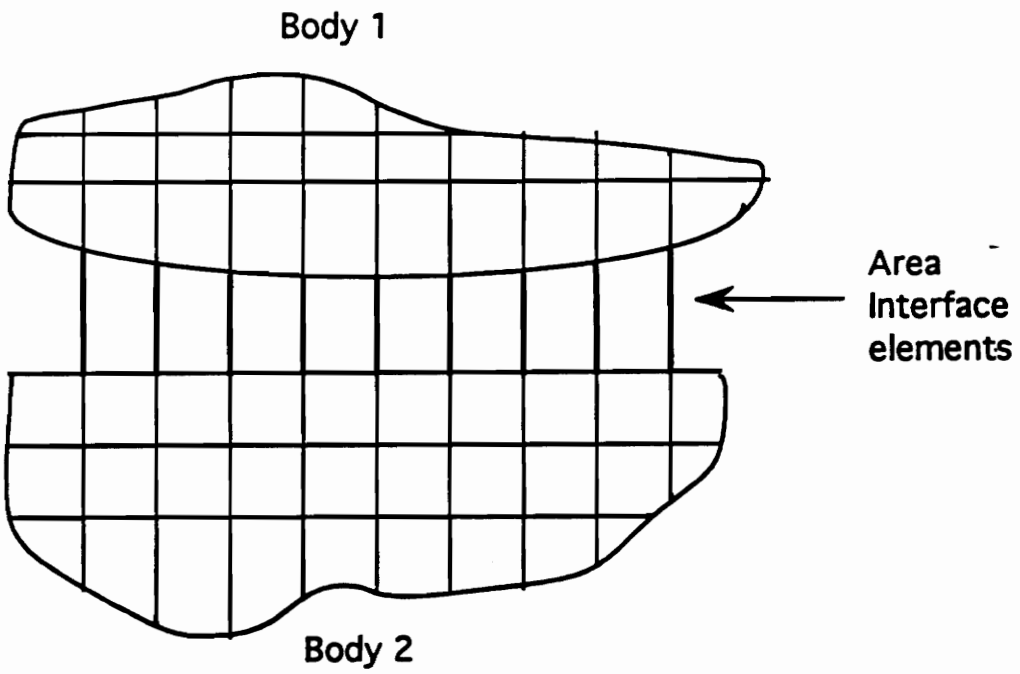

Figure 1.3. Two surfaces connected by area interface elements

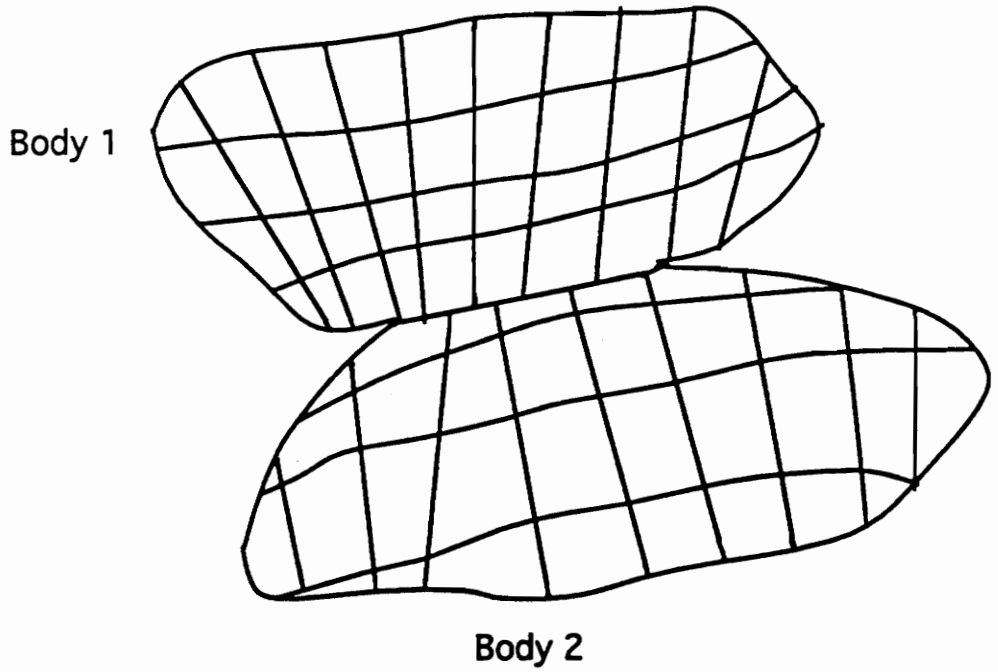

Figure 1.4. Two surfaces in slideline contact

of contact problems as it has clear advantages over the standard displacement method. First of all, since both displacements and stresses are nodal variables the boundary stresses or contact stresses can be obtained directly from the solution instead of postcomputing them from the strains. Secondly, the mixed finite element method yields the stresses directly at the boundary (the region of interest) while in the displacement based method they are obtained at the Gauss points and would have to be extrapolated to the boundary nodes. These succesive approximations might diminish the accuracy of the stresses in the displacement based method. Besides, the stresses might be required at intermediate steps of the analyses (for e.g. in geometrically non-linear analyses) and in such a case the stresses from the solution vector of the mixed finite element analysis can be directly used, thus saving time and retaining accuracy. For all these reasons the mixed finite element method would seem more preferable in contact analysis. In the current work a mixed finite element formulation based on the Hellinger-Reissner variational principle is used. For comparison and completeness a displacement based formulation is also included.

A literature review of finite element based contact analyses using the displacement method and the mixed finite element method is given below.

1.4 Literature review

A finite element technique to solve the frictionless contact problem using differential displacements was first presented by Wilson and Parsons[10]. They used the technique to solve problems in which statically indeterminate conditions arise as a result of the contact interface conditions. Chan and Tuba[11] treated the contact forces as unknowns and used iterative procedures to reach the assumed contact status. Ohte[12] solved the frictional contact problem as an extension of the work of Wilson and Parsons by incorporating the stick-slip conditions at the contact surface into the stiffness equation. Tsuta and Yamaji[13] formulated an

incremental stiffness equation that took into account the unknown forces at the contact surface and iteratively solved for the solution. Francavilla and Zienkiewicz[14] used a flexibility matrix in terms of contact pressures of the potential contact points to solve the frictionless contact problem. Gaertner[15] used triangular elements to solve the plane elastic contact problem with friction. Kalker[16] used variational principles and Campos, Oden and Kikuchi[17] solved the contact problem using non-linear inequalities. Okamoto and Nakazawa[18] used an incremental load approach to solve the frictional contact problem. Sachdeva and Ramakrishnan[19] modified the procedure of Francavilla and Zienkiewicz to include frictional effects at the contact surface. Oden and Pires[20] used the penalty method to solve frictional contact problems under nonlocal friction laws instead of the classical Coulombs law. Rahman[21] used an iterative technique along with a mixed coordinate system at the contact surface to solve the frictional contact problem. Chandrasekharan[22] proposed a new solution technique using geometric constraints to solve the progressive contact problem with friction. A penalty parameter was used to restore geometric compatibility at the contact nodes. Bathe and Chaudhary[23] imposed contact conditions by imposing stationarity of a modified functional obtained by adding the total potential due to contact forces for an element in contact to the original potential energy functional.

Studies using mixed finite elements are not as numerous as those using displacement elements. Tseng and Olson[24] used Reissner's principle to derive the mixed formulation from the equations of linear elasticity, for plane elastic contact. Haslinger and Hlavacek[25] presented a mixed formulation for the Signorini problem but gave no numerical results. Heyliger[26] developed a mixed variational statement using the updated Lagrangian formulation to analyse plane elastic contact problems. The variational statement was based on the Hellinger- Reissner variational principle. Two solution algorithms were presented to solve the contact problem with friction. The first one called the rigid pin algorithm is based on the iterative scheme developed by Rahman[21] and is used when one of the bodies is rigid. The

second, called the elastic pin algorithm is more general and is based on the idea developed by Bathe and Chaudhary for a displacement formulation.

1.5 Objective of the Present Study

The objective of the present work is to predict the contact stress distribution and variation of contact area with load in solid rocket motors. The motivation behind studying the contact problem in solid rocket motors is that it is the first step towards an impact analysis (a dynamic contact problem). The particular type of solid rocket motor structure considered is shown in Fig[1.5]. It is a layered cylinder and consists of a thin composite outer casing which covers a thick layer of propellant and a central air core. The composite case is orthotropic and has moduli much higher than the propellant. The cylindrical structure is assumed to be sufficiently long and so is analyzed as a plane strain problem.

The type of contact considered is progressive Hertzian type. An updated Lagrangian formulation (where all kinematic variables are refered to the previous configuration) is used along with a mixed variational statement based on the Hellinger-Reissner stationary principle. The mixed formulation yields two displacement and three stress components as nodal variables. The formulation is transformed so that the analysis is performed in cylindrical coordinates. This is necessary to satisfy the continuity of normal and shear components of stress at the nodes. The static condensation technique is used to condense out the discontinuous tangential stress components and after the solution is obtained they are computed at the element level. An algorithm based on the penalty method is developed to impose the contact constarints. A similar scheme was used by Chandrasekhar[22] for a displacement formulation. The technique which is a finite element adaptation of an optimization procedure for imposing equality constraints at discrete points is used to restore geometric compatibility at the contact surface.

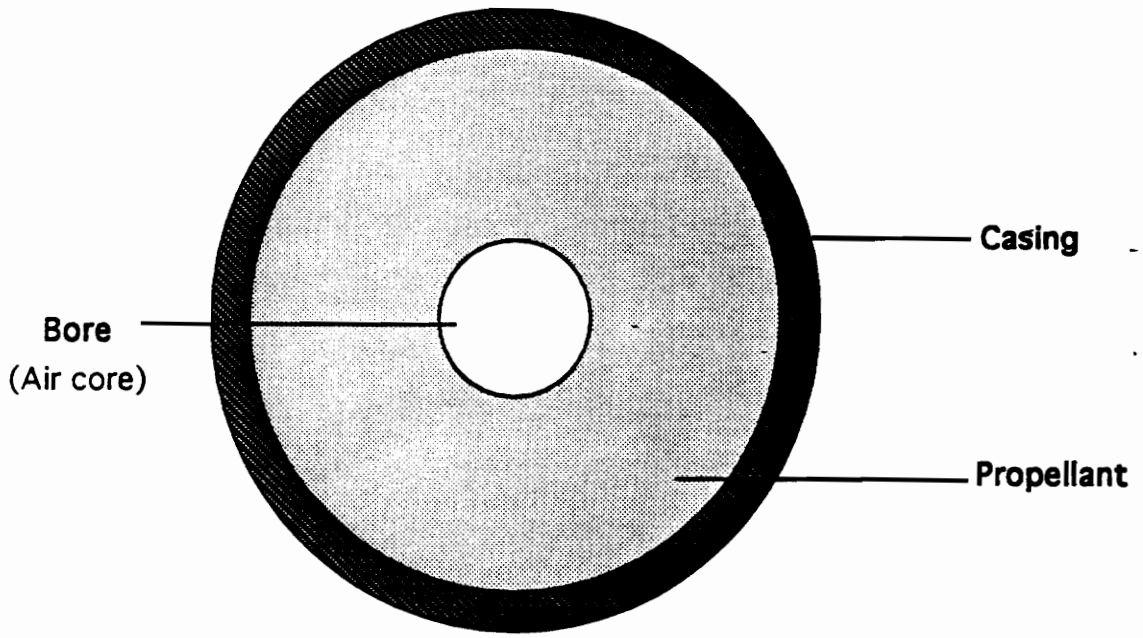

Figure 1.5. Schematic sketch of the solid rocket motor

The following chapters contain a detailed explanation of the topics introduced in this chapter. Chapter 2 deals with the development of the governing equations and the derivation of the mixed finite element models in two different coordinate systems. Chapter 3 introduces the penalty technique and contains a detailed description of the contact algorithm. Chapter 4 contains various numerical examples that were solved using the mixed finite element model and penalty technique. Chapter 5 gives a summary of the main topics dealt with in this work, the conclusions that were drawn from the results and the behaviour of the algorithm and recommendations for further extensions.

Chapter II

DEVELOPMENT OF GOVERNING EQUATIONS

2.1 Introduction

As described in Chapter 1, the contact problem is essentially nonlinear and as a result the assumption of infinitesimal displacements made in a linear analysis is not valid for accurate results. The continuous deformation of the body requires an appropriate incremental formulation to accomodate the consequences of finite deformations. These consequences will be outlined as the formulation is carried out. Of the two general incremental formulations, 'the total Lagrangian formulation', and the 'updated Lagrangian formulation', the latter will be adopted in the formulation to follow. In the updated Lagrangian formulation all the static and kinematic variables are referred to the previous configuration. The procedure is presented pictorially in Fig.[2.1].

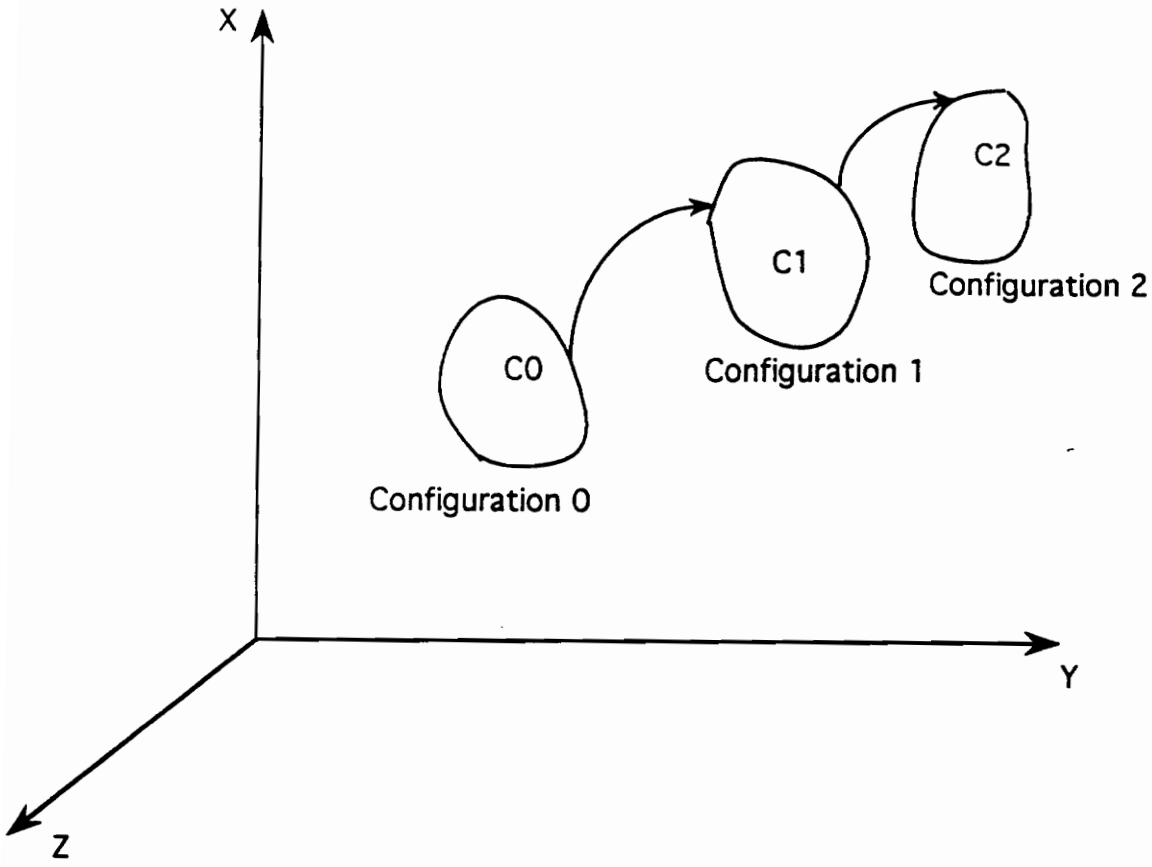

Figure 2.1. Motion of a body in cartesian coordinates

2.2 Equilibrium equations

In the incremental Lagrangian formulation of solids the equation of equilibrium is given by the principle of virtual work[27],

$$\int_{V_2} {}^2\tau_{ij}\ \delta({}^2e_{ij}) - \delta({}^2F)\ dV = 0 \tag{2.1}$$

where,

$$\delta({}^2F) = \int_{V_2} {}^2f_i\ \delta u_i\ dV + \int_{S_2} {}^2t_i\ \delta u_i\ dS \tag{2.2}$$

${}^2\tau_{ij}$ = components of the Cauchy stress tensor in configuration 2

${}^2e_{ij}$ = components of the strain tensor in configuration 2

$$= \frac{1}{2}\left(\frac{\partial u_i}{\partial X_j} + \frac{\partial u_j}{\partial X_i}\right)$$

${}^2f_i$ = cartesian components of the body force vector measured in configuration 2

${}^2t_i$ = cartesian components of the surface stress vector measured in configuration 2

u_i = components of the displacement vector

δ = variational operator

V_2 = volume of the body in configuration 2

S_2 = boundary of the body in configuration 2

Although equation 2.1 is applicable to the deformed configuration, it is not useful since the integration needs to be performed over a region that is not yet known. This is one of the consequences of not assuming infinitesimal deformations. The Cauchy stresses in the deformed configuration are also not known since they are defined as the force per unit area in current configuration. Hence we need to define auxiliary stress and strain measures which permit us to express the internal virtual work in equation (2.2) in terms of an integral that is known. There is another important reason to adopt auxiliary stress measures. Cauchy stresses in the deformed configuration cannot be obtained by simply adding stress increments that are due to straining of the material alone. This is because rigid body rotations which acting alone can change the components of the Cauchy stress tensor must also be accounted for in the calculation.

In order to represent the internal virtual work in the equation 2.1 in terms of an integral over a volume that is known and to facilitate incremental decomposition of the stresses and strains, auxiliary stress and strain measures are used[27]. A widely used stress measure in this regard is the second Piola-Kirchoff stress, which is defined as,

$$ {}^{2}_{1}S_{ij} = \frac{\rho_1}{\rho_2} \frac{\partial X_i}{\partial x_m} {}^{2}\tau_{mn} \frac{\partial X_j}{\partial x_n} \tag{2.3} $$

where,

ρ_1 = mass density in configuration 1

ρ_2 = mass density in configuration 2

X_j = coordinate in configuration 1

x_n = coordinate in configuration 2

${}^{2}\tau_{mn}$ = Cauchy stress tensor in configuration 2

In equation (2.3), ${}^{2}_{1}S_{ij}$ should be interpreted as the second Piola-Kirchoff stress at configuration 2 referred to configuration 1. Since by definition, the Cauchy stress tensor is measured in the most recent configuration, it follows that,

$$ {}^{2}_{2}S_{ij} = {}^{2}\tau_{ij} \tag{2.4} $$

We also define the Green-Lagrange strain tensor as,

$$ {}^{2}_{1}E_{ij} = \frac{1}{2}\left(\frac{\partial u_i}{\partial X_j} + \frac{\partial u_j}{\partial X_i} + \frac{\partial u_m}{\partial X_i}\frac{\partial u_m}{\partial X_j}\right) \tag{2.5} $$

where ${}^{2}_{1}E_{ij}$ is the Green lagrange strain tensor in configuration 2 referred to configuration 1· and,

u_i = components of displacement vector

X_i = coordinates in configuration 1

The variation of the Green-Lagrange strain tensor E_{ij} is related to the variation of the infinitesimal strain tensor e_{ij} by the following transformation,

$$ \delta({}^{2}_{1}E_{ij}) = \frac{\partial x_m}{\partial X_i}\frac{\partial x_n}{\partial X_j}\,\delta({}^{2}e_{mn}) \tag{2.6} $$

For a proof of relation 2.6, see reference [27].

From equation 2.1 we have,

$$\int_{V_2} {}^2\tau_{ij}\ \delta({}^2e_{ij}) = \int_{V_2} \frac{\rho_2}{\rho_1}\ \frac{\partial x_i}{\partial X_m}\ {}^2_1S_{mn}\ \frac{\partial x_j}{\partial X_n}\ \frac{\partial X_m}{\partial X_n}\ \frac{\partial X_k}{\partial x_i}\ \frac{\partial X_l}{\partial x_j}\ \delta({}^2_1E_{kl})\ dV$$
$$= \int_{V_2} \frac{\rho_2}{\rho_1}\ {}^2_1S_{mn}\ \delta({}^2_1E_{mn})\ dV \qquad (2.7)$$

In writing equation (2.7), the identity $\frac{\partial x_i}{\partial X_m}\ \frac{\partial X_k}{\partial x_i} = \delta_{mk}$ has been used.

Assuming no change in the mass density of the body, that is, $\rho_2\, dV_2 = \rho_1\, dV_1$, we get,

$$\int_{V_1} {}^2_1S_{ij}\ \delta({}^2_1E_{ij})\ dV = \int_{V_2} {}^2\tau_{ij}\ \delta({}^2e_{ij})\ dV \qquad (2.8)$$

Equation 2.8 also demonstrates that the second Piola-Kirchoff stress tensor is energetically conjugate to the Green-Lagrange strain tensor just as the Cauchy stress tensor is energetically conjugate to the infinitesimal strain tensor.

Substituting equation 2.8 into the equation for internal virtual work given by equation 2.1 and assuming that applied loading is independent of the deformation of the structure, that is,

$$\delta({}^2F) = \delta({}^1F) \qquad (2.9)$$

we obtain,

$$\int_{V_1} {}^2_1S_{ij}\ \delta({}^2_1E_{ij})\ dV - \delta({}^1F) = 0 \qquad (2.10)$$

This equation is in terms of the known configuration, that is, C_1

The incremental decompositions of the stresses and strains are given by,

$$ {}^{2}_{1}S_{ij} = {}^{1}\tau_{ij} + {}_{1}S_{ij} \tag{2.11a} $$

$$ {}^{2}_{1}E_{ij} = {}_{1}e_{ij} + {}_{1}\eta_{ij} \tag{2.11b} $$

where,

${}_{1}S_{ij}$ = incremental component of 2nd Piola-Kirchoff stress tensor

${}_{1}e_{ij}$ = incremental component of the linear strain tensor

$$ = \frac{1}{2}\left(\frac{\partial u_i}{\partial X_j} + \frac{\partial u_j}{\partial X_i}\right) $$

${}_{1}\eta_{ij}$ = incremental component of the nonlinear strain tensor

$$ = \frac{1}{2}\left(\frac{\partial u_m}{\partial X_i}\ \frac{\partial u_m}{\partial X_j}\right) $$

It is clear from the above relations that the Cauchy stress at configuration 2 is equal to the second Piola-Kirchoff stress at configuration 2. This also follows from the definition of Cauchy stress.

Substituting 2.9 and 2.10 into 2.8 we obtain,

$$ \int_{V_1} ({}^{1}\tau_{ij} + {}_{1}S_{ij})\ \delta({}_{1}e_{ij} + {}_{1}\eta_{ij})\, dV - \delta({}^{1}F) = 0 \tag{2.12} $$

Equation 2.12 can be written as,

$$ \int_{V_1} {}_{1}S_{ij}\, \delta({}_{1}e_{ij} + {}_{1}\eta_{ij})\ dV + \int_{V_1} {}^{1}\tau_{ij}\, \delta({}_{1}\eta_{ij})\, dV $$

$$= -\int_{V_1} {}^1\tau_{ij}\ \delta({}_1e_{ij})\ dV + \delta({}^1F) \tag{2.13}$$

Equation 2.13 can be written as,

$$\int_{V_1} {}_1C_{ijrs}\ {}_1e_{rs}\ \delta({}_1e_{ij})\ dV + \int_{V_1} {}^1\tau_{ij}\ \delta({}_1\eta_{ij})\ dV = -\int_{V_1} {}^1\tau_{ij}\ \delta({}_1e_{ij})\ dV + \delta({}^1F) \tag{2.14}$$

wherein the linearization, ${}_1S_{ij} = {}_1C_{ijrs}\ e_{rs}$ and $\delta\hat{E}_{ij} = \delta_1e_{ij}$ has been used in writing the first term.

Equation 2.14 represents the approximate total potential energy in configuration 2 but referred to configuration 1. The mixed finite element model is now constructed by introducing the strain displacement relations into the above variational statement as constraints and by using the increment in the second Piola-Kirchoff stress tensor as a Lagrange multiplier. We then obtain a modified functional which is given as,

$$\Pi_M = \Pi + \int_{V_1} \left[\ \frac{1}{2}\ \{u_{i,j} + u_{j,i}\}\ - {}_1e_{ij}\ \right]\ {}_1S_{ij}\ dV \tag{2.15}$$

The Hellinger-Reissner stationary variational principle is now given by setting $\delta\Pi_M = 0$,

$$\begin{aligned}\delta(\Pi_M) = \int_{V_1} \delta(\frac{1}{2}\ C_{ijkl}\ {}_1e_{ij}\ {}_1e_{kl} - {}_1S_{ij}\ {}_1e_{ij}) + {}^1\tau_{ij}\ \delta_1e_{ij} \\ + {}^1\tau_{ij}\ {}_1\eta_{ij} + \frac{1}{2}\ \delta({}_1S_{ij}\ u_{i,j}) + \frac{1}{2}\ \delta({}_1S_{ij}\ u_{j,i})\ dV - \delta(F_1) = 0\end{aligned} \tag{2.16}$$

The first term of equation 2.16 can be written as,

$$\begin{aligned}\delta\left(\frac{1}{2}\,{}_1S_{kl}\,D_{klij}\,{}_1S_{ij} - {}_1S_{ij}\,D_{ijkl}\,{}_1S_{kl}\right) &= \delta\left(-\frac{1}{2}\,D_{ijkl}\,S_{ij}\,S_{kl}\right)\\ &= -\frac{1}{2}\left(D_{ijkl}\,{}_1S_{ij}\,\delta_1S_{kl} + D_{ijkl}\,\delta_1S_{ij}\,{}_1S_{kl}\right)\\ &= -\frac{1}{2}\left(D_{klij}\,{}_1S_{kl}\,\delta_1S_{ij} + D_{ijkl}\,\delta_1S_{ij}\,{}_1S_{kl}\right)\\ &= -D_{ijkl}\,{}_1S_{kl}\,\delta_1S_{ij}\end{aligned} \tag{2.17}$$

Substituting in equation 2.16 we get,

$$\int_{V_1}\left[-D_{ijkl}\,{}_1S_{kl}\,\delta_1S_{ij} + {}^1\tau_{ij}\,\delta({}_1e_{ij}\,{}_1\eta_{ij}) + \delta\{{}_1S_{ij}\,\frac{1}{2}\,(u_{i,j}+u_{j,i})\}\right]dV - \delta F_1 = 0 \tag{2.18}$$

Imposing stationarity with respect to displacements,

$$\int_{V_1}\left[{}^1\tau_{ij}\,\delta(e_{ij}+\eta_{ij}) + \frac{1}{2}\,{}_1S_{ij}\,\delta(u_{i,j}+u_{j,i})\right]dV - \delta F_1 = 0 \tag{2.19}$$

Using symmetry of the stress tensor S_{ij} the above equation can be written as,

$$\int_{V_1}\left[{}_1\tau_{ij}\,\delta(e_{ij}+\eta_{ij}) + {}_1S_{ij}\,\delta(u_{i,j})\right]dV = \delta F_1 \tag{2.20}$$

Imposing stationarity with respect to stresses,

$$\int_{V_1}\left[u_{i,j}\,\delta_1S_{ij} - D_{ijkl}\,S_{kl}\,\delta S_{ij}\right]dV_1 = 0 \tag{2.21}$$

We thus obtain the two governing equations,

$$\int_{V_1} [\, {}^1\tau_{ij}\, \delta(e_{ij} + \eta_{ij}) \;+\; {}_1S_{ij}\, \delta(u_{i,j})] \; dV \;=\; \delta F_1 \tag{2.22a}$$

$$\int_{V_1} [\, u_{i,j}\, \delta_1 S_{ij} \;-\; D_{ijkl}\; {}_1S_{kl}\; \delta_1 S_{ij} \,]\, dV \;=\; 0 \tag{2.22b}$$

Wherein

$${}^2_1S_{ij} \;=\; {}^1\tau_{ij} \;+\; {}_1S_{ij} \tag{2.23a}$$

$${}^2_1u_i \;=\; {}^1u_i \;+\; u_i \tag{2.23b}$$

Since the equations 2.22 were obtained by linearization, they are only an approximation of the true equation of equilibrium. Hence they must be solved simultaneously until the increments in stresses and displacements lie within a small prescribed tolerance. Hence, within a prescribed load step we need to solve for the solution vector iteratively.

Before deriving the finite element model, a note about the nature of the mixed finite element solution is in order. The displacement based finite element method, which is based on the principle of minimization of total potential energy starts off by assuming approximate displacement functions. The functional is then expressed in terms of the approximate model and the minimization generates governing equations that are approximate. But the compatibility conditions are satisfied identically. In the force or stress finite element model, which is based on the principle of minimum complementary energy, approximate stress functions are assumed to establish the approximate functional. This formulation yields governing relations that satisy the equilibrium equations identically but only satisfy the compatibility conditions approximately. A mixed finite element model, which is based on a stationary principle rather than a minimization of energy, embodies the satisfaction of both the equilibrium equations and compatibility conditions since the equlibrium equations, stress-strain relations, strain-

displacement equations and the essential boundary conditions are all taken into consideration in deriving the governing equations.

2.3 Finite element model

In this section the two dimensional finite element model is constructed from the governing equations 2.22. In the mixed finite element model, the displacements and stresses are approximated independently in the following form,

$$u_i(x,y,z) = \Sigma\ u_j\ \psi_j(x,y,z) \tag{2.24a}$$

$$S_{ij}(x,y,z) = \Sigma\ S_{ij}^{k}\ \psi_k(x,y,z) \tag{2.24b}$$

Although the same symbol ψ_i has been used in equations 2.24 for the interpolation functions for displacements and stresses it is to be understood that in general they can be different. This also follows from the fact that in the mixed model we approximate the displacements and stresses independently. However, there are certain rules to be followed in the selection of the order of the approximating functions and this is discussed in detail in a subsequent section. Substituting these expressions into the governing equations 2.22, we obtain,

$$\begin{bmatrix} [K^{11}] & [0] & [K^{13}] & [0] & [K^{15}] \\ [0] & [K^{22}] & [0] & [K^{24}] & [K^{25}] \\ [K^{31}] & [0] & [K^{33}] & [K^{34}] & [K^{35}] \\ [0] & [K^{42}] & [K^{43}] & [K^{44}] & [K^{45}] \\ [K^{51}] & [K^{52}] & [K^{53}] & [K^{54}] & [K^{55}] \end{bmatrix} \begin{bmatrix} \{u\} \\ \{v\} \\ \{S_{xx}\} \\ \{S_{yy}\} \\ \{S_{xy}\} \end{bmatrix} = \begin{bmatrix} \{F_x^L\} \\ \{F_y^L\} \\ \{0\} \\ \{0\} \\ \{0\} \end{bmatrix} - \begin{bmatrix} \{F_x^{NL}\} \\ \{F_y^{NL}\} \\ \{0\} \\ \{0\} \\ \{0\} \end{bmatrix} \tag{2.25}$$

where,

$\{u\}$ = vector of incremental displacements in X-direction

$\{v\}$ = vector of incremental displacements in Y-direction

$\{S_{xx}\}$ = vector of incremental stresses in X-direction

$\{S_{yy}\}$ = vector of incremental stresses in Y-direction

$\{S_{xy}\}$ = vector of incremental shear stresses

$\{F_x^L\}$ = linear force vector in X-direction

$\{F_y^L\}$ = linear force vector in Y-direction

$\{F_x^{NL}\}$ = nonlinear force vector in X-direction

$\{F_y^{NL}\}$ = nonlinear force vector in Y-direction

and the components of the stiffness matrix and force vectors are given by,

$$K_{ij}^{11} = \int_{V_1} \left[\tau_{xx} \left(\frac{\partial \psi_i}{\partial x} \frac{\partial \psi_j}{\partial x} \right) + \tau_{yy} \left(\frac{\partial \psi_i}{\partial y} \frac{\partial \psi_j}{\partial y} \right) + \tau_{xy} \left(\frac{\partial \psi_i}{\partial x} \frac{\partial \psi_j}{\partial y} + \frac{\partial \psi_i}{\partial y} \frac{\partial \psi_j}{\partial x} \right) \right] dx\, dy$$

$$K_{ij}^{22} = K_{ij}^{11}$$

$$K_{ij}^{13} = \int_V \frac{\partial \psi_i}{\partial x} \psi_j \, dx\, dy = K_{ji}^{31}$$

$$K_{ij}^{15} = \int_V \frac{\partial \psi_i}{\partial y} \psi_j \, dx\, dy = K_{ji}^{51}$$

$$K_{ij}^{24} = \int_V \frac{\partial \psi_i}{\partial y} \psi_j \, dx\, dy = K_{ji}^{42}$$

$$K_{ij}^{25} = \int_V \frac{\partial \psi_i}{\partial x} \psi_j \, dx \, dy = K_{ji}^{52}$$

$$K_{ij}^{33} = -\int_V D_{11} \psi_i \, \psi_j \, dx \, dy$$

$$K_{ij}^{44} = -\int_V D_{22} \psi_i \, \psi_j \, dx \, dy$$

$$K_{ij}^{55} = -\int_V D_{66} \psi_i \, \psi_j \, dx \, dy$$

$$K_{ij}^{34} = -\int_V D_{12} \psi_i \, \psi_j \, dx \, dy = K_{ji}^{43}$$

$$K_{ij}^{35} = -\int_V D_{16} \psi_i \, \psi_j \, dx \, dy = K_{ji}^{53}$$

$$K_{ij}^{45} = -\int_V D_{26} \psi_i \, \psi_j \, dx \, dy = K_{ji}^{54}$$

$$\{F_x^L\} = \int_V f_x \psi_i \, dx \, dy + \int_\Gamma (\tau_{xx} n_x + \tau_{xy} n_y) \psi_i \, dS$$

$$\{F_y^L\} = \int_V f_y \psi_i \, dx \, dy + \int_\Gamma (\tau_{xy} n_x + \tau_{yy} n_y) \psi_i \, dS$$

$$\{F_x^{NL}\} = \int_V (\tau_{xx} \frac{\partial \psi_i}{\partial x} + \tau_{xy} \frac{\partial \psi_i}{\partial y}) \, dx \, dy$$

$$\{F_y^{NL}\} = \int_V (\tau_{yy} \frac{\partial \psi_i}{\partial y} + \tau_{xy} \frac{\partial \psi_i}{\partial x}) \, dx \, dy$$

2.3.1 On solving the positive indefinite mixed finite element matrices

It can be seen from the expression for the submatrix $[K^{11}]$ in equation (2.25) that it depends on the values of Cauchy stresses evaluated in the previous iteration. Hence, in the first iteration of the first load step the submatrix $[K^{11}]$ will contain all zeros since the Cauchy stresses are all zero throughout the domain of the body in the undeformed configuration. If the element matrix is assembled as it is, the global stiffness matrix will also contain zeros corresponding to its contribution from the submatrix $[K^{11}]$. This would make the stiffness matrix positive indefinite since zeros will appear on the principal diagonal and a conventional solver will be useless for this system of equations. Using a solver with partial pivoting will circumvent the problem, but such a procedure would destroy the bandedness of the stiffness matrix and would increase the computational cost. An alternative procedure used by Mirza [28] and Yogeswaran et. al.[29] was to multiply and divide the global stiffness matrix by its transpose. This made the global stiffness matrix positive definite and also preserved the banded character of the matrix. In the present work, a simpler procedure was adopted since it also suited the geometry of the problem. Both the displacement components corresponding to the first node of the finite element mesh were constrained in both the coordinate directions. This would cause a *1* to be placed on the principal diagonal corresponding to the first and second degrees of freedom. This is the way in which the imposition of essential boundary conditions proceeds in the finite element program [9]. Now any conventional banded solver can be used since the 1's are now used as the pivots and any further zeros on the diagonal will not affect the solution process. Hence, the positive indefinite nature of the mixed finite element matrix is overcome

using a specific node numbering procedure. Another point that merits mention is that although from the first two equations of 2.25 it appears as if the two displacement components are decoupled, the Poisson effect is taken care of by the fifth equation.

2.4 Finite element model in cylindrical coordinates

In the mixed finite element method the displacements and stresses are approximated independently over an element. If all the degrees of freedom are retained and assembled globally, they are also forced to be continuous at the nodes. While displacements are almost always continuous, the stresses may not be. This situation arises when the material of the body is discontinuous. It is clear from the fundamentals of mechanics that the normal and shear stresses will be continuous but not the tangential stress component. It is also evident that it is difficult to enforce the continuity of the normal and shear components in the cartesian coordinate system. For this reason, the formulation of section 2.3 has been transformed into the cylindrical coordinate system. This formulation also facilitates the imposition of stress boundary conditions (for e.g. one may wish to explicitly impose stress free boundary conditions on free boundaries of the structure).

Since the tangential component of stress will be discontinuous across different material boundaries, it must not be assembled globally but must be condensed out at the element level. This is achieved by the well known static condensation technique which is demonstrated in the later portion of this section.

The formulation in terms of cylindrical coordinates is obtained by substituting into eqns (2.22) the equivalent components of strain in cylindrical coordinates and simultaneously transforming the stress components. Since the algebra involved in this process is quite tedious, only the

results are reproduced below. After performing the requisite transformations, the following finite element model is obtained,

$$\begin{bmatrix} [K_{11}] & [K_{12}] & [K_{13}] & [K_{14}] & [K_{15}] \\ [K_{21}] & [K_{22}] & [0] & [K_{24}] & [K_{25}] \\ [K_{31}] & [0] & [K_{33}] & [K_{34}] & [0] \\ [K_{41}] & [K_{42}] & [0] & [K_{44}] & [0] \\ [K_{51}] & [K_{52}] & [0] & [0] & [K_{55}] \end{bmatrix} \begin{bmatrix} \{u_r\} \\ \{u_\theta\} \\ \{S_{rr}\} \\ \{S_{\theta\theta}\} \\ \{S_{r\theta}\} \end{bmatrix} = \begin{bmatrix} \{F_r^L\} \\ \{F_\theta^L\} \\ \{0\} \\ \{0\} \\ \{0\} \end{bmatrix} - \begin{bmatrix} \{F_r^{NL}\} \\ \{F_\theta^{NL}\} \\ \{0\} \\ \{0\} \\ \{0\} \end{bmatrix} \tag{2.26}$$

where,

$\{u_r\}$ = vector of incremental displacements in radial direction

$\{u_\theta\}$ = vector of incremental displacements in tangential direction

$\{S_{rr}\}$ = vector of incremental radial stresses

$\{S_{\theta\theta}\}$ = vector of incremental tangential stresses

$\{S_{r\theta}\}$ = vector of incremental shear stresses

$\{F_r^L\}$ = linear force vector in radial direction

$\{F_\theta^L\}$ = linear force vector in tangential direction

$\{F_r^{NL}\}$ = nonlinear force vector in radial direction

$\{F_\theta^{NL}\}$ = nonlinear force vector in tangential direction

and the components of the stiffness matrix and force vectors are given by,

$$K_{ij}^{11} = \int_{\Omega} \tau_{rr} \frac{\partial \psi_i}{\partial r} \frac{\partial \psi_j}{\partial r} + \tau_{\theta\theta} \frac{1}{r^2} \left(\frac{\partial \psi_i}{\partial \theta} \frac{\partial \psi_j}{\partial \theta} + \frac{1}{r^2} \psi_i \psi_j \right) + \tau_{r\theta} \frac{1}{r} \left(\frac{\partial \psi_i}{\partial r} \frac{\partial \psi_\theta}{\partial \theta} + \frac{1}{r} \frac{\partial \psi_i}{\partial \theta} \frac{\partial \psi_j}{\partial r} \right) r \, dr \, d\theta$$

$$K_{ij}^{22} = K_{ij}^{11}$$

$$K_{ij}^{12} = \int_{\Omega} \left[{}^1\tau_{r\theta} \left(\frac{1}{r} \psi_i \frac{\partial \psi_j}{\partial r} - \frac{1}{r} \frac{\partial \psi_i}{\partial r} \psi_j \right) + {}^1\tau_{\theta\theta} \left(\frac{1}{r^2} \psi_i \frac{\partial \psi_j}{\partial \theta} - \frac{1}{r^2} \frac{\partial \psi_i}{\partial \theta} \psi_j \right) \right] r \, dr \, d\theta = K_{ji}^{21}$$

$$K_{ij}^{13} = \int_{\Omega} \left[\frac{\partial \psi_i}{\partial r} \psi_j \right] r \, dr \, d\theta = K_{ji}^{31}$$

$$K_{ij}^{14} = \int_{\Omega} \left[\frac{1}{r} \psi_i \psi_j \right] r \, dr \, d\theta = K_{ji}^{41}$$

$$K_{ij}^{15} = \int_{\Omega} \left[\frac{1}{r} \frac{\partial \psi_i}{\partial \theta} \psi_j \right] r \, dr \, d\theta = K_{ji}^{51}$$

$$K_{ij}^{23} = K_{ji}^{32} = 0$$

$$K_{ij}^{24} = \int_{\Omega} \left[\frac{1}{r} \frac{\partial \psi_i}{\partial \theta} \psi_j \right] r \, dr \, d\theta = K_{ji}^{42}$$

$$K_{ij}^{25} = \int_{\Omega} \left[\frac{\partial \psi_i}{\partial r} \psi_j - \psi_i \psi_j \frac{1}{r} \right] r \, dr \, d\theta = K_{ji}^{52}$$

$$K_{ij}^{33} = - \int_{\Omega} D_{11} \psi_i \psi_j \, r \, dr \, d\theta$$

$$K_{ij}^{34} = -\int_{\Omega} D_{12}\,\psi_i\,\psi_j\,r\,dr\,d\theta$$

$$K_{ij}^{35} = -\int_{\Omega} D_{16}\,\psi_i\,\psi_j\,r\,dr\,d\theta$$

$$K_{ij}^{43} = -\int_{\Omega} D_{21}\,\psi_i\,\psi_j\,r\,dr\,d\theta$$

$$K_{ij}^{44} = -\int_{\Omega} D_{22}\,\psi_i\,\psi_j\,r\,dr\,d\theta$$

$$K_{ij}^{45} = -\int_{\Omega} D_{26}\,\psi_i\,\psi_j\,r\,dr\,d\theta$$

$$K_{ij}^{53} = -\int_{\Omega} D_{61}\,\psi_i\,\psi_j\,r\,dr\,d\theta$$

$$K_{ij}^{54} = -\int_{\Omega} D_{62}\,\psi_i\,\psi_j\,r\,dr\,d\theta$$

$$K_{ij}^{55} = -\int_{\Omega} D_{66}\,\psi_i\,\psi_j\,r\,dr\,d\theta$$

$$\{F_r^L\} = \int_{\Omega} f_r\,\psi_i\,r\,dr\,d\theta + \int_{\Gamma} \{\tau_{rr}\,n_r + \tau_{r\theta}\,n_\theta\}\,ds$$

$$\{F_r^{NL}\} = -\int_\Omega \left[\tau_{rr}\frac{\partial \psi_i}{\partial r} + \frac{\tau_{r\theta}}{r}\frac{\partial \psi_i}{\partial \theta} + \tau_{\theta\theta}\frac{\psi_i}{r}\right] r\,dr\,d\theta$$

$$\{F_\theta^L\} = \int_\Omega f_\theta\,\psi_i\,r\,dr\,d\theta + \int_\Gamma \{\tau_{r\theta}\,n_r + \tau_{\theta\theta}\,n_\theta\}\,ds$$

$$\{F_\theta^{NL}\} = -\int_\Omega \left[\tau_{r\theta}\left\{\frac{\partial \psi_i}{\partial r} - \frac{1}{r}\,\psi_i\right\} + \tau_{\theta\theta}\,\frac{1}{r}\,\frac{\partial \psi_i}{\partial \theta}\right] r\,dr\,d\theta$$

2.5 Static condensation

As mentioned earlier, in the case of a solid rocket motor, the material properties are not the same throughout the structure. Typically, a thick layer of soft propellant is enclosed in a hard outer casing. As a result, the tangential stress component will not be continuous and needs to be condensed out at the element level. This is necessitated because of the mixed formulation approach wherein both displacements and stresses are approximated independently and consequently appear as nodal variables. The process of condensing out the tangential stress reduces the global degrees of freedom per node to four from five.

The equations 2.26 can be written as,

$$[K^{11}]\{u_r\} + [K^{12}]\{u_\theta\} + [K^{13}]\{S_{rr}\} + [K^{14}]\{S_{\theta\theta}\} + [K^{15}]\{S_{r\theta}\} = \{F_r\} \qquad (2.27a)$$

$$[K^{21}]\{u_r\} + [K^{22}]\{u_\theta\} + [K^{23}]\{S_{rr}\} + [K^{24}]\{S_{\theta\theta}\} + [K^{25}]\{S_{r\theta}\} = \{F_\theta\} \qquad (2.27b)$$

$$[K^{31}]\{u_r\} + [K^{32}]\{u_\theta\} + [K^{33}]\{S_{rr}\} + [K^{34}]\{S_{\theta\theta}\} + [K^{35}]\{S_{r\theta}\} = \{0\} \qquad (2.27c)$$

$$[K^{41}]\{u_r\} + [K^{42}]\{u_\theta\} + [K^{43}]\{S_{rr}\} + [K^{44}]\{S_{\theta\theta}\} + [K^{45}]\{S_{r\theta}\} = \{0\} \qquad (2.27d)$$

$$[K^{51}]\{u_r\} + [K^{52}]\{u_\theta\} + [K^{53}]\{S_{rr}\} + [K^{54}]\{S_{\theta\theta}\} + [K^{55}]\{S_{r\theta}\} = \{0\} \quad (2.27e)$$

where,

$$\{F_r\} = \{F_r^L\} - \{F_r^{NL}\}$$

$$\{F_\theta\} = \{F_\theta^L\} - \{F_\theta^{NL}\}$$

From equation (2.27d),

$$\{S_{\theta\theta}\} = -[K^{44}]^{-1}[K^{41}]\{u_r\} - [K^{44}]^{-1}[K^{42}]\{u_\theta\} - [K^{44}]^{-1}[K^{43}]\{S_{rr}\} - [K^{44}]^{-1}\{S_{r\theta}\} \quad (2.28)$$

Substituting this in equations (2.27a), (2.27b), (2.27c) and (2.27e) we get,

$$\begin{bmatrix} [SK11] & [SK12] & [SK13] & [SK14] \\ [SK21] & [SK22] & [SK23] & [SK24] \\ [SK31] & [SK32] & [SK33] & [SK34] \\ [SK41] & [SK42] & [SK43] & [SK44] \end{bmatrix} \begin{bmatrix} \{u_r\} \\ \{u_\theta\} \\ \{S_{rr}\} \\ \{S_{r\theta}\} \end{bmatrix} = \begin{bmatrix} \{F_r\} \\ \{F_\theta\} \\ \{0\} \\ \{0\} \end{bmatrix} \quad (2.29)$$

where,

$$[SK11] = [K^{11}] - [K^{14}][K^{44}]^{-1}[K^{41}]$$

$$[SK12] = [K^{12}] - [K^{14}][K^{44}]^{-1}[K^{42}]$$

$$[SK13] = [K^{13}] - [K^{14}][K^{44}]^{-1}[K^{43}]$$

$$[SK14] = [K^{15}] - [K^{14}][K^{44}]^{-1}[K^{45}]$$

$$[SK21] = [K^{21}] - [K^{24}][K^{44}]^{-1}[K^{41}]$$

$$[SK22] = [K^{22}] - [K^{24}][K^{44}]^{-1}[K^{42}]$$

$$[SK23] = [K^{23}] - [K^{24}][K^{44}]^{-1}[K^{43}]$$

$$[SK24] = [K^{25}] - [K^{24}][K^{44}]^{-1}[K^{45}]$$

$$[SK31] = [K^{31}] - [K^{34}][K^{44}]^{-1}[K^{41}]$$

$$[SK32] = [K^{32}] - [K^{34}][K^{44}]^{-1}[K^{42}]$$

$$[SK33] = [K^{33}] - [K^{34}][K^{44}]^{-1}[K^{43}]$$

$$[SK34] = [K^{35}] - [K^{34}][K^{44}]^{-1}[K^{45}]$$

$$[SK41] = [K^{51}] - [K^{54}][K^{44}]^{-1}[K^{41}]$$

$$[SK42] = [K^{52}] - [K^{54}][K^{44}]^{-1}[K^{42}]$$

$$[SK53] = [K^{53}] - [K^{54}][K^{44}]^{-1}[K^{43}]$$

$$[SK54] = [K^{55}] - [K^{54}][K^{44}]^{-1}[K^{45}]$$

2.6 On the nature of mixed approximations

As has been mentioned earlier, in the mixed finite element method, the displacements and stresses are approximated independently. In this section, some important considerations concerning the nature of these approximations will be mentioned and discussed.

It is known from the finite element theory that the approximating functions must satisfy certain conditions. These are, (i) the approximating functions should be sufficiently differentiable (ii)

the set of approximating functions should be complete and linearly independent and (iii) the approximating functions should satisfy at least the homogeneous form of the essential boundary conditions. The differentiability criterion is decided by looking at the differentiability required of the dependent variables in the variational statement or the weak form of the governing differential equations. Performing this procedure for the equations (2.22) we see that the displacement components are each differentiated once with respect to each of the coordinate directions and that the stress components are undifferentiated. Thus, the stresses should be approximated by at least a constant and the displacement components by at least a bilinear function (linear in both the coordinate directions). The respective approximations should also be consistent with the mathematical definition relating stress and displacement (that is, stresses are a function of the gradient of the displacement).

The above discussion is usually valid for standard finite element approximations. However, the requirements mentioned in the earlier paragraph are not sufficient when using mixed finite elements. There are further restrictions on the order of the polynomials approximating the stresses and displacements. If these restrictions are violated, the solution leads to mechanisms and non-unique solutions. Mirza and Olson [30] have performed extensive studies on this aspect and have proposed a completeness criterion which is reproduced below:

" *The strains from the stress approximations should possess at least all the strain modes that are present in the strains derived from the displacement approximations.*"

The purport of the above statement is that unless the stress and displacement approximations are of a given order, the element matrices will contain more than the allowable three zero eigenvalues corresponding to the three rigid body modes for two-dimensional bodies. Mirza et. al. performed an eigenvalue analysis of the mixed element matrix for various combinations of interpolations for displacements and stresses in a rectangular element. They found that the correct three zero eigenvalues for the expected rigid body modes are obtained only when the order of the approximating functions for displacements and stresses are the same. Their re-

sults are reproduced in Table [2.1]. That is, only bilinear-bilinear, biquadratic-biquadratic combinations are allowable. When other combinations were used, more than three zero eigenvalues were obtained and the stresses in the eigenvectors for these extra zero eigenvalues were always zero. These extra modes are mechanisms since they cause an apparent strain without any stress. Also, these mechanisms cannot be eliminated by imposing essential boundary conditions.

In keeping with the guidelines mentioned above, only linear-linear combinations of approximating functions for the displacements and stresses respectively have been used in this work.

Table 2.1. Eigenvalues for different interpolation orders

Interpolation		Degrees of Freedom			Sign of Eigen-values	No. of Eigen-values	Composition of Eigenvectors
u,v	$\tau_{xx},\tau_{yy},\tau_{xy}$	u,v	τ's	Total			
Bilinear	Constant	8	3	11	(-)	3	τ's constant; u,v bilinear
					(0)	5**	τ's=0;($u_{,x}=v_{,y}=u_{,y}+v_{,x}=0$;u,v bilinear).
					(+)	3	τ's constant; u,v bilinear.
Bilinear	Bilinear	8	12	20	(-)	12	τ's,u,v bilinear.
					(0)	3†	τ's=$u_{,x}=v_{,y}=u_{,y}+v_{,x}=0$.†
					(+)	5	τ's,u,v bilinear.
Biquadratic*	Bilinear	16	12	28	(-)	12	τ's bilinear; u,v biquadratic.
					(0)	4**	τ's=0;($u_{,x}=v_{,y}=u_{,y}+v_{,x}=0$;u,v biquadratic).
					(+)	12	τ's bilinear; u,v biquadratic.
Biquadratic	Biquadratic	16	24	40	(-)	24	τ's,u,v biquadratic.
					(0)	3	τ's=$u_{,x}=v_{,y}=u_{,y}+v_{,x}=0$.
					(+)	13	τ's,u,v biquadratic.

* Full quadratic in x and y plus x^2y and xy^2.

** Extra zero eigenvalues are associated with mechanisms which have the same u,v distributions as the approximating polynomials.

† Rigid body modes ($u_{,x}=0;v_{,y}=0;u_{,y}+v_{,x}=0$).

(Reproduced from the paper by Mirza and Olson [30])

Chapter III

NUMERICAL ALGORITHM FOR CONTACT CONSTRAINT

3.1 Introduction

In this chapter the technique used to analyze the planar contact problem will be outlined. While a number of techniques have been used in the past to analyze contact problems, most of them are quite complicated and utilize a number of iterative schemes to account for the changing boundary conditions at the contact surface. Typically, constraints have been imposed by the use of Lagrange multipliers. This method suffers from the inconvenience of increasing the number of unknown parameters to be solved for. It also yields indefinite matrices (especially in linear problems) and special procedures need to be adopted to overcome this difficulty.

The following sections explain an alternative technique and algorithm that is effective in imposing the contact constraints and also converges in a couple of iterations. The algorithm is

based on a finite element adaptation of an optimization technique[22], the penalty function method. This method avoids the difficulties associated with the Lagrange multipliers mentioned above.

3.2 General concepts

The penalty function method is an optimization technique which allows the reformulation of a constrained variational problem as one without constraints. For example, consider the functional F(x,y) subject to the equality constraint G(x,y).

$$F(x,y) = f(x,y) \tag{3.1}$$

subject to the constraint,

$$G(x,y) = 0 \tag{3.2}$$

This problem can be reformulated by using the modified functional,

$$F_L(x,y) = f(x,y) + \frac{\gamma}{q}[G(x,y)]^q \tag{3.3}$$

wherein γ is a preassigned weight parameter called the penalty parameter. The effect of the second term on the right side is to increase the functional F_L in proportion to the $q\,th$ power of the amount by which the constraints are violated. That is, there is a penalty for violating the constraints and the amount of penalty for violating the constraints increases at a faster rate compared to the amount of violation of a constraint. It can be seen that for sufficiently large values of the penalty parameter γ, the solution to equation (3.3) will be close to the actual solution. If γ is a very large positive constant, then a minimum is obtainable only if the product $\gamma\,[G]^q$ is small and hence minimizing F_L is equivalent to minimizing a function not

substantially different from $F(x,y)$ while ensuring that the constraint is nearly satisfied. Although in general any value of q greater than one can be used, in practice the value $q = 2$ is used. It can be seen from eqn. (3.3) that this ensures that the constraints are satisfied in a least square sense.

Although the penalty method seems to be best suited for situations where a minimum of F(x,y) is sought, it is equally applicable to situations where F(x,y) is stationary. The process is equally applicable to constraints applied on boundaries as simple discrete constraints. It is in this latter form that the penalty method is used in the present work.

3.3 Selection of penalty parameter

In the earlier section it was said that as the value of the penalty parameter is increased, the solution becomes more accurate. This is because, as the magnitude of the penalty parameter γ is increased, satisfaction of the constraints is imposed more closely. However, in practice the upper limit on the penalty parameter depends on the computer used. If the absolute magnitude of the elements of a coefficient matrix (in our case the global stiffness matrix), vary by a large amount, truncation and round-off errors can be large. These errors are a function of the number of digits used to represent a given number (that is, the word length of the computer). With the advent of powerful computers and double precision arithemetic, this is no longer much of a problem. The actual selection of a value could be an empirical one or as a thumb rule, one can adopt a value that is about a couple of orders of magnitudes greater than the largest entry in the global stiffness matrix.

3.4 Tracking and imposing contact constraints

Consider two bodies A_1 and A_2 brought together by the application of imposed displacements or tractions Fig.[3.1]. In the present analysis we will assume that one of the bodies, say A_1 is rigid and the other A_2 is deformable. This assumption simplifies the imposition of contact constraints and is also consistent with the specific problem under study. The basic technique is however quite general and can be extended to the case where both the bodies are deformable.

For the sake of clarity let A_1 be the indentor body and A_2 be the target body. On the application of load, the two bodies come into contact and contact forces develop in the region of contact Fig.[3.2]. The contact stresses and contact area are both unknown in this region of contact Fig.[3.3]. However, at the instant when a node just touches the surface the contact pressure is zero. This leaves the contact area as the only unknown at that instant. The area of contact can only be determined after a node has made contact. Hence it is necessary to keep track of all potential contacting nodes in deciding when actually the contact overlap occurs. Then kinematic constraints in the form of the impenetrability condition is imposed to restore compatibility, thus establishing the contact area. The impenetrability condition states that no part of either body can lie within the other. The procedure by which the contact overlap is detected and compatibility restored is illustrated below.

The procedure will be described for the case of the Hertzian or progressive contact problem which is also the type of contact problem of interest in the present work. In this type of contact, successive nodes come into contact as the load is increased. We assume that there is no contact at the initial configuration C_1. The stationarity of the Hellinger-Reissner variational principle yields finite element equations of the form,

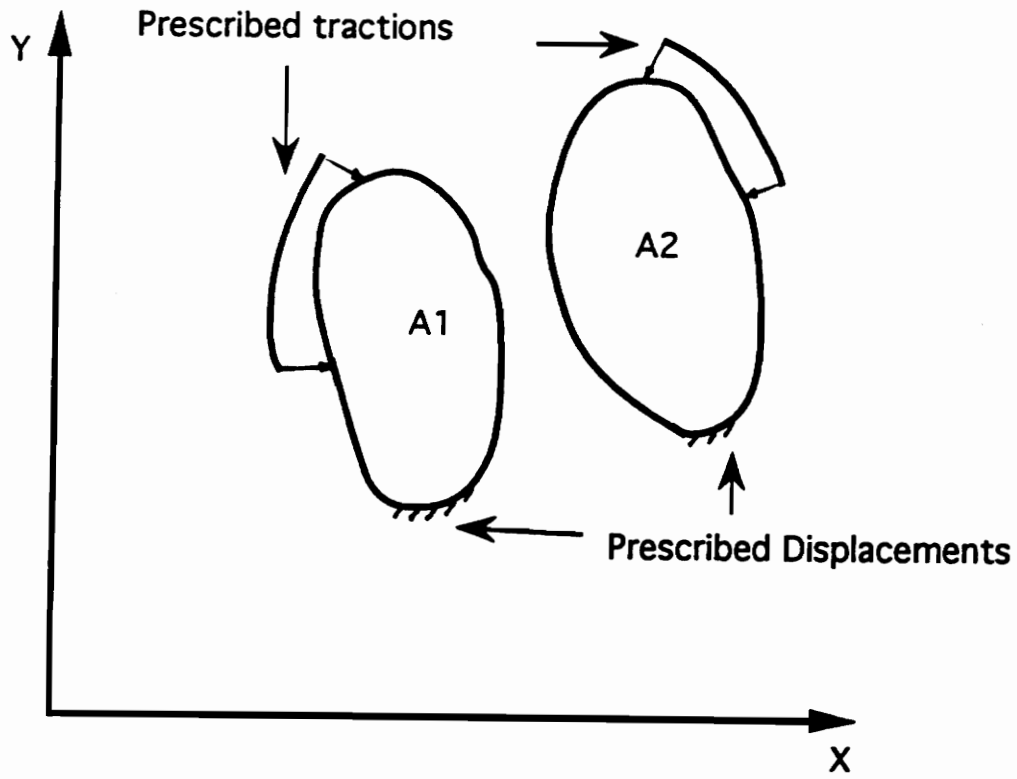

Figure 3.1. Two bodies to be brought into contact

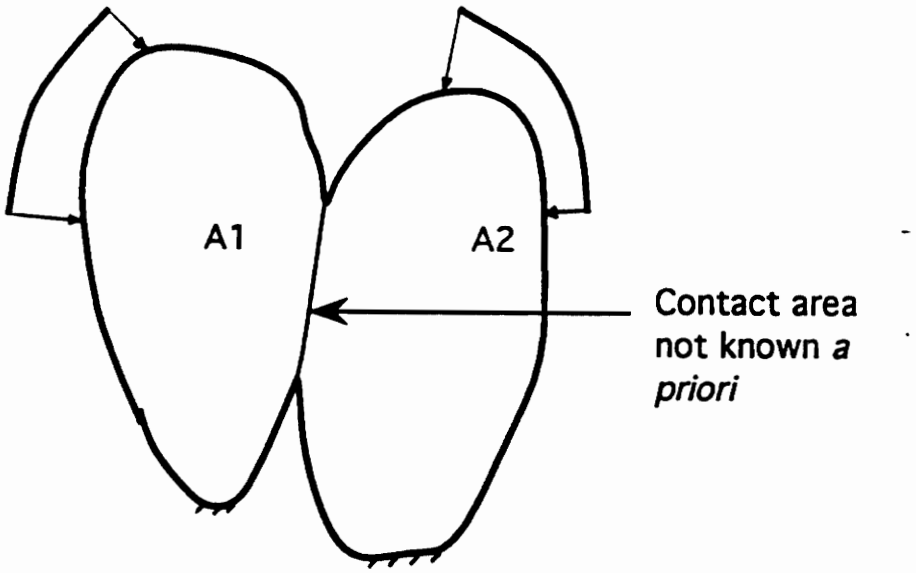

Figure 3.2. Configuration of the two bodies at contact

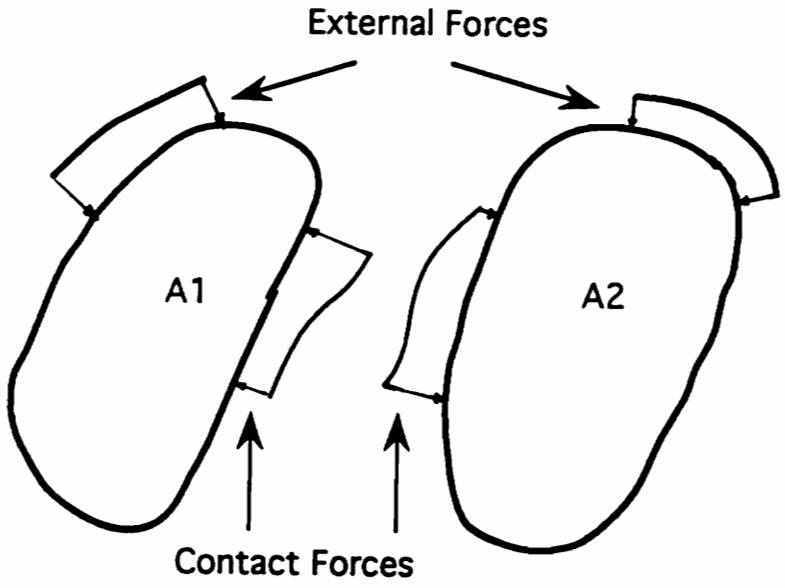

Figure 3.3. Forces acting on the two bodies in contact

$$[K_L + K_{NL}] \begin{bmatrix} \Delta u \\ \Delta S \end{bmatrix} = [\Delta F] \tag{3.4}$$

wherein K_L is the linear stiffness matrix and K_{NL} is the nonlinear stiffness matrix due to geometric or material nonlinearities, and,

$$^{2}_{1}u_i = {}_1u_i + \Delta u_i \tag{3.5a}$$

$$^{2}_{1}S_{ij} = {}_1S_{ij} + \Delta S_{ij} \tag{3.5b}$$

are the incremental decompositions of the displacements and stresses.

Since equilibrium is satisfied and no contact is made between bodies A_1 and A_2 compatibility and force equilibrium are both satisfied at configuration C_1. Let an additional load step be taken such that the new configuration is C_2. The motion of the nodes can be represented by,

$$^{2}\vec{X}_m = {}^{1}\vec{X}_m + \Delta u_m \vec{i} + \Delta v_m \vec{j}\ , \quad m = 1,2....N \tag{3.6}$$

wherein N is the total number of global nodes. The incremental motion from configuration 1 to 2 can be represented by,

$$\vec{X} = {}^{2}\vec{X}_m - {}^{1}\vec{X}_m \tag{3.7}$$

If the load increments are small this linear displacement path can be considered acceptable. If the compatibility is violated at any external surface, that is, between bodies A_1 and A_2, then the equilibrium equation (3.4) does not satisfy compatibility. This kinematic violation is shown in Fig.[3.4].

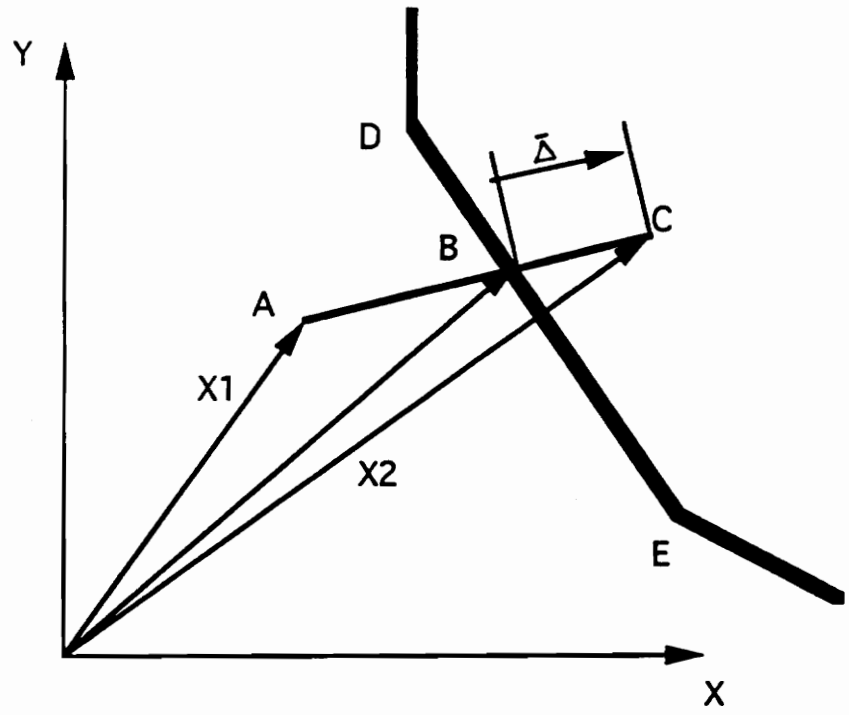

A : initial position of the node *m*
C : position of node *m* after penetration
B : final position of node *m*
Δ : overlap

Figure 3.4. Violation of compatibility and contact overlap

Since the current positions of the potential contact nodes are being constantly monitored, the contact point B can be determined as soon as a contact overlap is detected. Numerically, the contact overlap is given by,

$$\begin{aligned}\vec{\Delta} &= ({}^2\vec{X}_C - \vec{X}_B) \\ &= x_m\vec{i} + y_m\vec{j}\end{aligned} \tag{3.8}$$

where x_m and y_m are the penetrations of the node m in the X and Y directions respectively.

In order to achieve kinematic compatibility, sufficient force must be applied at node m in configuration C to bring it to B. Equivalently, a displacement of $-\vec{\Delta}$ can be applied to C. The displacement of $-(x_m\vec{i} + y_m\vec{j})$ is obtained in this work using the penalty function method. The finite element equation in configuration 2 can be written as,

$$\begin{bmatrix} K_{11} & K_{12} & K_{13} & \cdots & & & & \\ \cdots & \cdots & \cdots & \cdots & & & & \\ & & & & & & & \\ & & & & K_{pp} & & & \\ & & & & \cdots & K_{qq} & & \\ & & & & & \cdots & \cdots & \\ & & & & & & & K_{nn} \end{bmatrix} \begin{bmatrix} \Delta u_1 \\ \Delta v_1 \\ \Delta S_{11} \\ \cdots \\ \Delta u_p \\ \Delta v_p \\ \cdots \\ \Delta S_{nn} \end{bmatrix} = \begin{bmatrix} \Delta F_1 \\ \Delta F_2 \\ \Delta F_3 \\ \cdots \\ \Delta F_p \\ \Delta F_q \\ \cdots \\ \Delta F_n \end{bmatrix} \tag{3.9}$$

where p and q are the global degrees of freedom at node m. Now let,

$$\tilde{K}^i_{pp} = \gamma K^i_{pp} \tag{3.10a}$$

and

$$\Delta F^i_p = \Delta F^{(i-1)}_p + x_m \tilde{K}^i_{pp} \tag{3.10b}$$

where i is the iteration number, K_{pp} appearing on the right hand side is the nominal stiffness obtained in the finite element formulation. K_{pp} on the left hand side is the modified stiffness to be used in equation (3.9). Similarly, for the qth degree of freedom,

$$\tilde{K}^{I}_{qq} = \gamma K^{I}_{qq} \tag{3.11a}$$

and

$$\Delta F^{I}_{q} = \Delta F^{(i-1)}_{q} + y_m \tilde{K}^{I}_{qq} \tag{3.11b}$$

It should be clear from the similarity to the earlier discussion on penalty methods that the second term of equations (3.10b) and (3.11b) represent the constraint to be satisfied. In our case they represent the incremental displacements to be achieved at the node in the given direction. γ is the penalty parameter.

Physically, the above penalty method can be interpreted as equivalent to adding a spring of large stiffness at node m and applying a load that results in the desired displacement level.

3.4 Description of the algorithm

In this section, a step by step description of the solution strategy and the computational details are discussed. We will consider the case of the Hertz contact problem to describe the steps. Extensions to the layered cylinder problem only require performing the static condensation and calculations in cylindrical coordinates.

Step 1: The potential contact nodes along the boundary are computed and stored in a matrix $NCONT(I)$. The value of the penalty parameter γ is also initialised.

Step 2: The load loop is begun. The load is applied incrementally such that not more than one node comes into contact during that step. The number of load steps are controlled by a user supplied parameter *LS* .

Step 3: The iteration loop for both force imbalance and contact is started. This means that the contact status is checked in every iteration of each load step.

Step 4: The stiffness matrices are assembled and the incremental finite element solution $\{GF\}$ is obtained. The total solution matrix $\{GF1\}$ is updated.

Step 5: The convergence is checked using the Euclidean norm of the total solution. Since the solution contains both displacements and stresses, each is checked separately.

Step 6: If the solution converges, go to Step 10. If the solution does not converge, the previous solution and geometry are stored. The geometry is then updated to obtain the most current deformed configuration. This is equivalent to,

$$x(i) = x(i) + \Delta u_i$$

$$y(i) = y(i) + \Delta v_i$$

where, $i = 1.....N$, N being the total number of global nodes and x and y are the coordinates.

Step 7: The coordinates of the potential contact nodes are checked in the most current configuration for possible penetration. A counter *ICONT(I)* is activated to keep track of any nodes that may have overlapped.

Step 8: If a node, say m has overlapped, the amount of overlap is calculated using equation (3.8). This calculation is possible only because we have assumed a linear motion of the node from the immediate previous configuration to the present position.

Step 9: Control is passed back to Step 3. After the global stiffness is assembled for the new iteration, the nominal stiffnesses corresponding to the *m*th degree of freedom are modified according to equations (3.10) and (3.11). The solution is then checked for convergence.

Step 10: Print the solution and proceed to next load step i.e. Step 1.

When dealing with frictionless problems, the node that has been pushed to the surface should be free to move in the tangential direction and should be restrained only in the vertical or normal directions to the two surfaces. Hence, in Step 9, equation (3.10) and equation (3.11) should both be imposed only in the first iteration after contact overlap is detected. After that only the equation that corresponds to the degree of freedom that might cause penetration on further loading should be used. This would free the node to move along the target surface but not penetrate it.

Chapters 2 and 3 involved the construction of the formulation and the development of the contact algorithm respectively. In Chapter 4, the algorithm will used to solve numerical problems and its accuracy will be checked against known classical solutions.

Chapter IV

NUMERICAL PROBLEMS AND RESULTS

4.1 Introduction

In this chapter, different numerical examples are chosen to verify and validate the effectiveness of using a mixed formulation combined with a penalty based method for contact constraints. Wherever possible finite element solutions are compared with analytical solutions or other numerical solutions. Throughout the solution procedures, fully nonlinear(geometric) mixed formulations have been used. The sensitivity of the contact algorithm to steep changes in the material properties from one layer to the other is also investigated.

4.2 Hertz contact problem

In this section, an overview of the classical Hertz problem is given before using this analytical solution to compare with the finite element solution. The problem involving two elastic cylin-

ders of different radii in contact was first solved by Heinrich hertz in 1882 [2]. The Hertzian theory relies on the basic assumption that the highly concentrated contact stress can be treated separately from the general distribution of stress in the contacting bodies. The general stress distribution may arise because of the shape of the bodies or due to the way in which they are supported. For the above assumption to hold, the following conditions need to be satisfied : (1) the contact area must be small compared with the dimensions of each body and with the relative radii of curvature of the surfaces and (2) the surfaces are frictionless. Using these assumptions, the following Hertzian formulae have been derived for the two dimensional contact of cylindrical bodies. For a discussion of the theoretical and mathematical details, refs.[4][5] can be consulted. The formulae alone are reproduced below,

$$E^D = \left[\frac{1 - \nu_1^2}{E_1} + \frac{1 - \nu_2^2}{E_2} \right]^{-1} \tag{4.1}$$

where,

ν_i = Poissons ratio of cylinder i, $i = 1,2$

E_i = Youngs modulus of cylinder i, $i = 1,2$

$$R = \left[\frac{1}{R_1} + \frac{1}{R_2} \right]^{-1} \tag{4.2}$$

where,

R_i = radius of curvature of cylinder i, $i = 1,2$

For a line load of P per unit length, maximum contact pressure is given by,

$$p_{max} = \left[\frac{P E^D}{\pi R} \right]^{\frac{1}{2}} \tag{4.3}$$

Semi-contact width b is given by,

$$b = \left[\frac{4PR}{\pi E^D} \right]^{\frac{1}{2}} \tag{4.4}$$

Pressure distribution as a function of distance from centreline is given by,

$$p(x) = \frac{E^D}{2R} \left[\frac{4PR}{\pi E^D} - x^2 \right]^{\frac{1}{2}} \tag{4.5}$$

where x is the distance from the centerline.

4.3 Finite element solution for the Hertz contact problem

The schematic of the contact problem that is modeled is shown in Fig[4.1]. An elastic cylinder pressed against a rigid half-space is idealized as a plane strain problem by assuming that the cylinder is very long. Only a quarter of the cylinder is modeled by exploiting the symmetry in the problem. The Youngs Modulus of the cylinder is 21000 Psi and the Poissons ratio is 0.3. The radius is 1.0 inches. Tha material values mentioned above were not adopted for any specific reason other than to compare with earlier published results [31].

Two different finite element meshes are used to idealize the problem. The first is a coarse mesh Fig.[4.2] which uses 66 isoparametric linear elements. The number of degrees of freedom is 410. The load is applied as a point force at the center of the cylinder. At the maximum load of 248 lb/in, four nodes make the contact with the rigid surface. The deformed mesh is shown in Fig.[4.3]. The results of the analysis for the coarse mesh are shown in Figs[4.4] and [4.5]. The numerical results are compared with the Hertz analytical solutions given by equations (4.1)-(4.5) wherein $R_2 = \infty$ and $E_2 = \infty$ need to be substituted to model the rigid half-space. Fig.[4.4] shows the contact pressure distribution as a function of the distance from

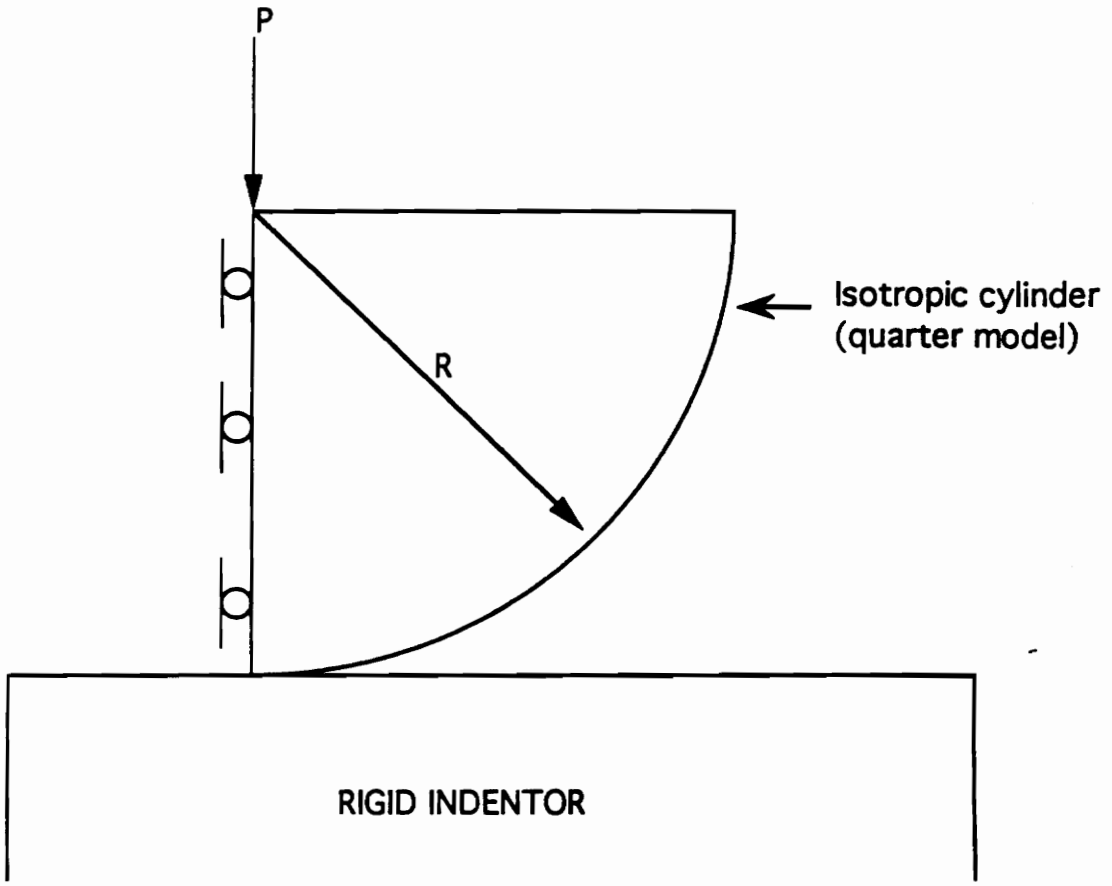

Figure 4.1. Schematic of the Hertz contact problem

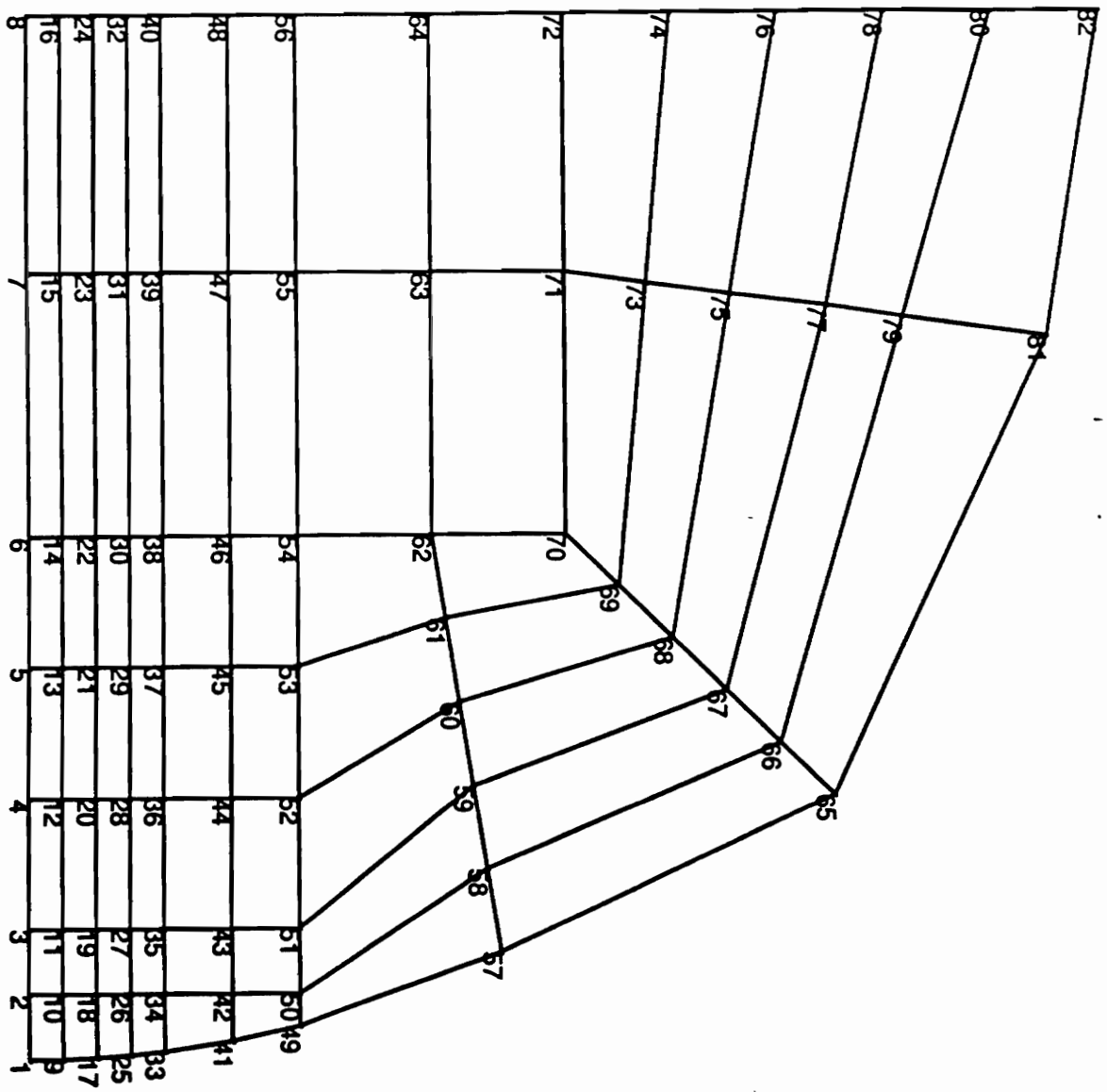

Figure 4.2. Coarse finite element mesh for the Hertz contact problem

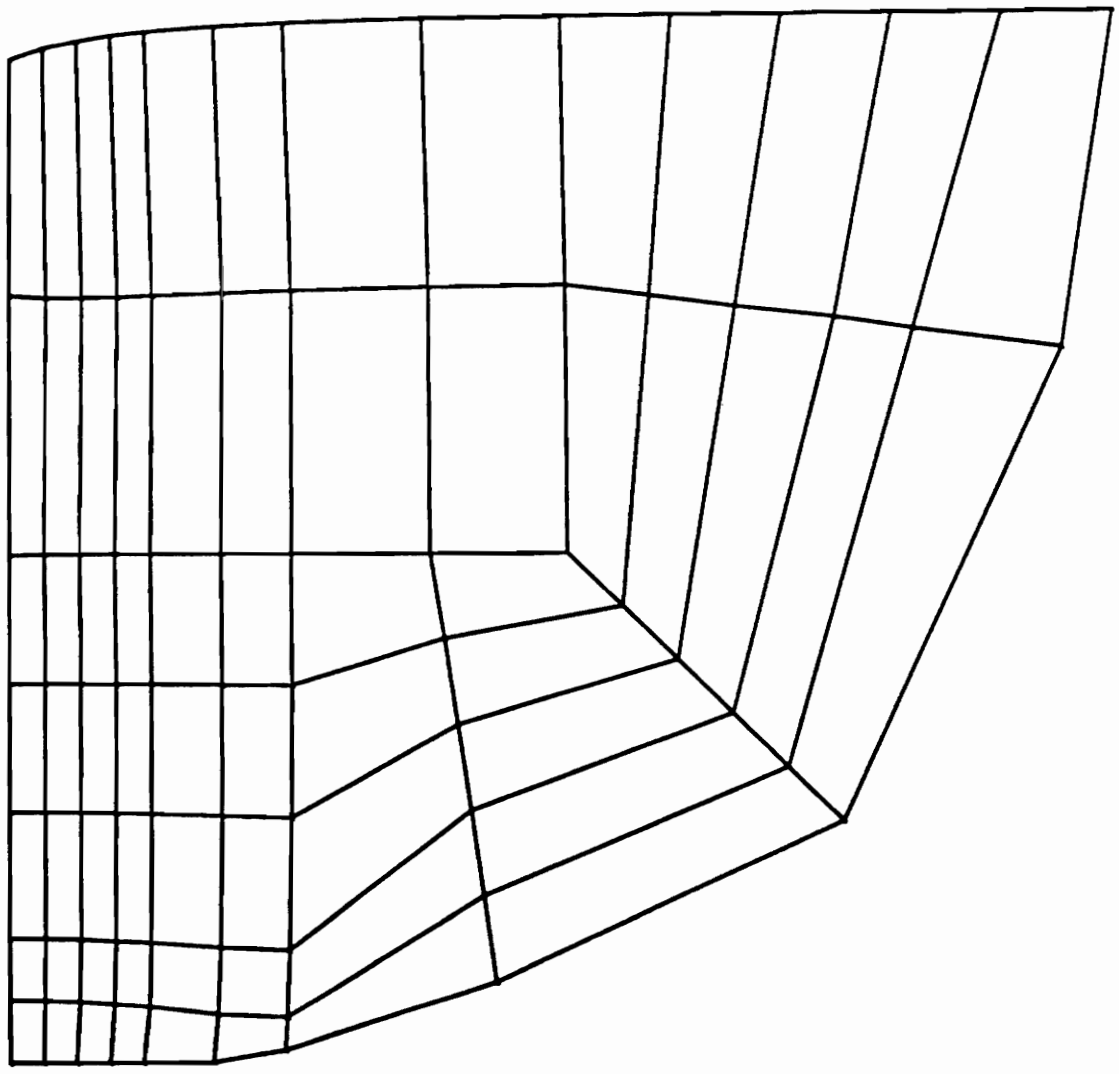

Figure 4.3. Deformed configuration (4 nodes in contact) for the coarse mesh

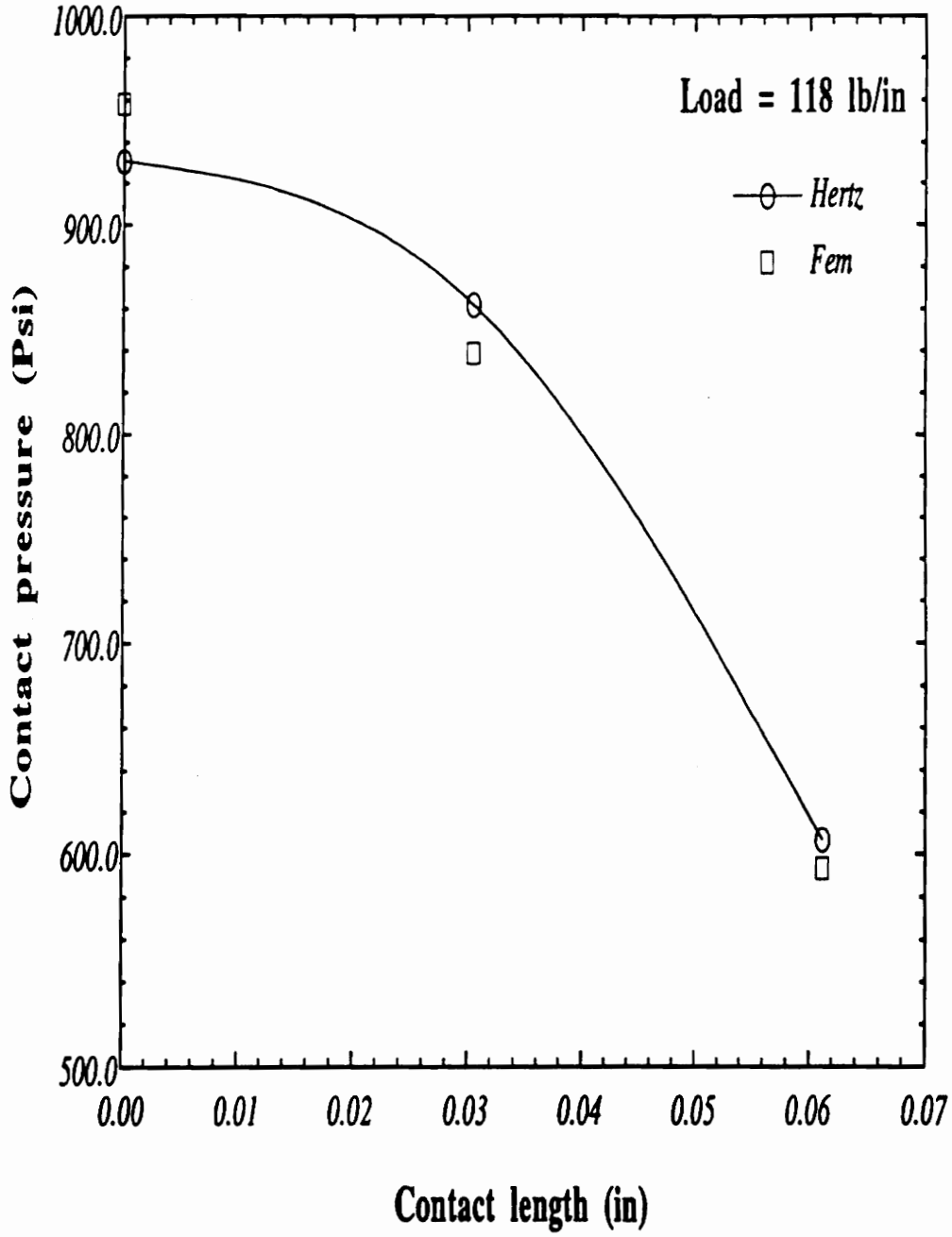

Figure 4.4. Contact pressure vs centreline distance for a load of 118 lb/in

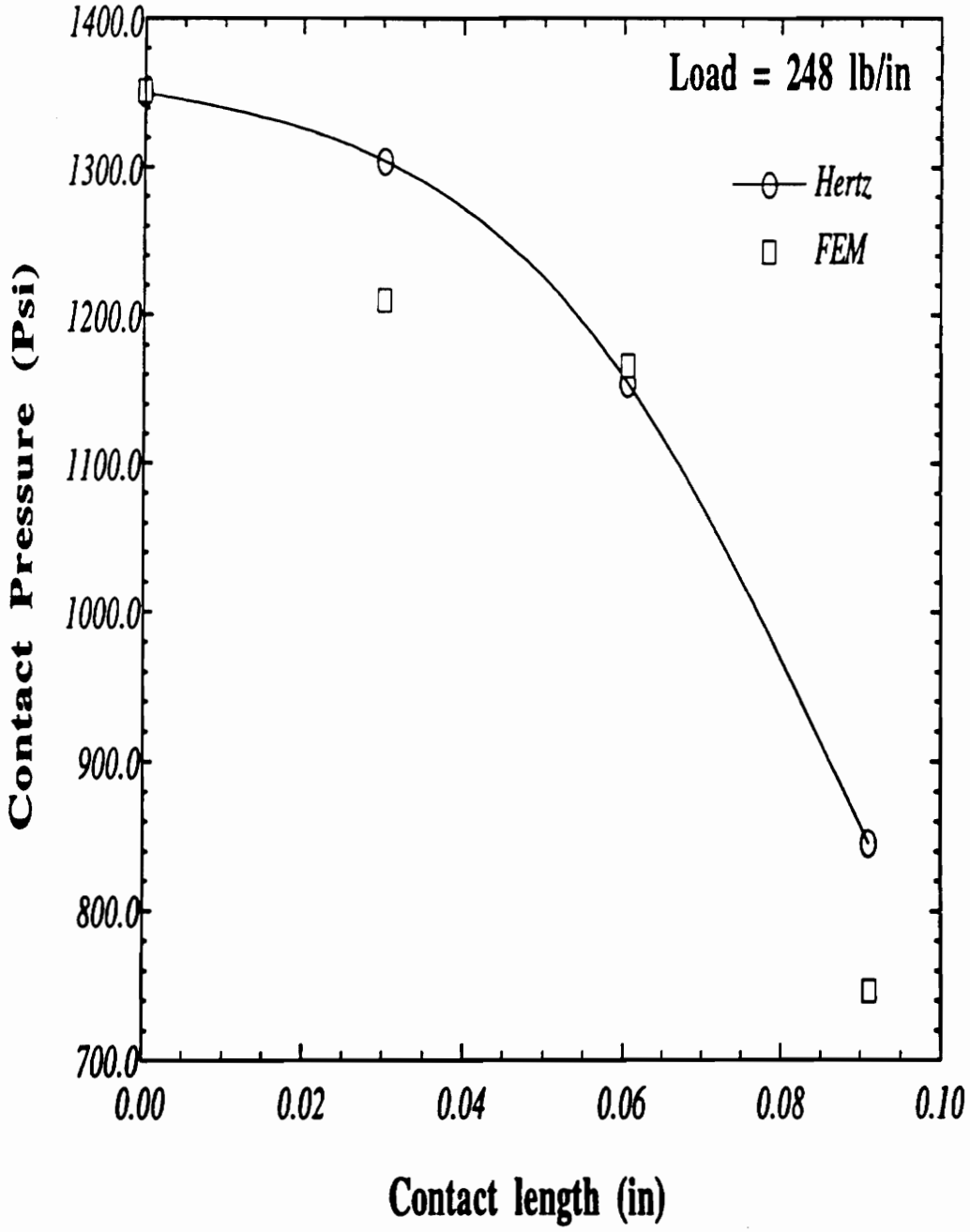

Figure 4.5. Contact pressure vs centreline distance for a load of 248 lb/in

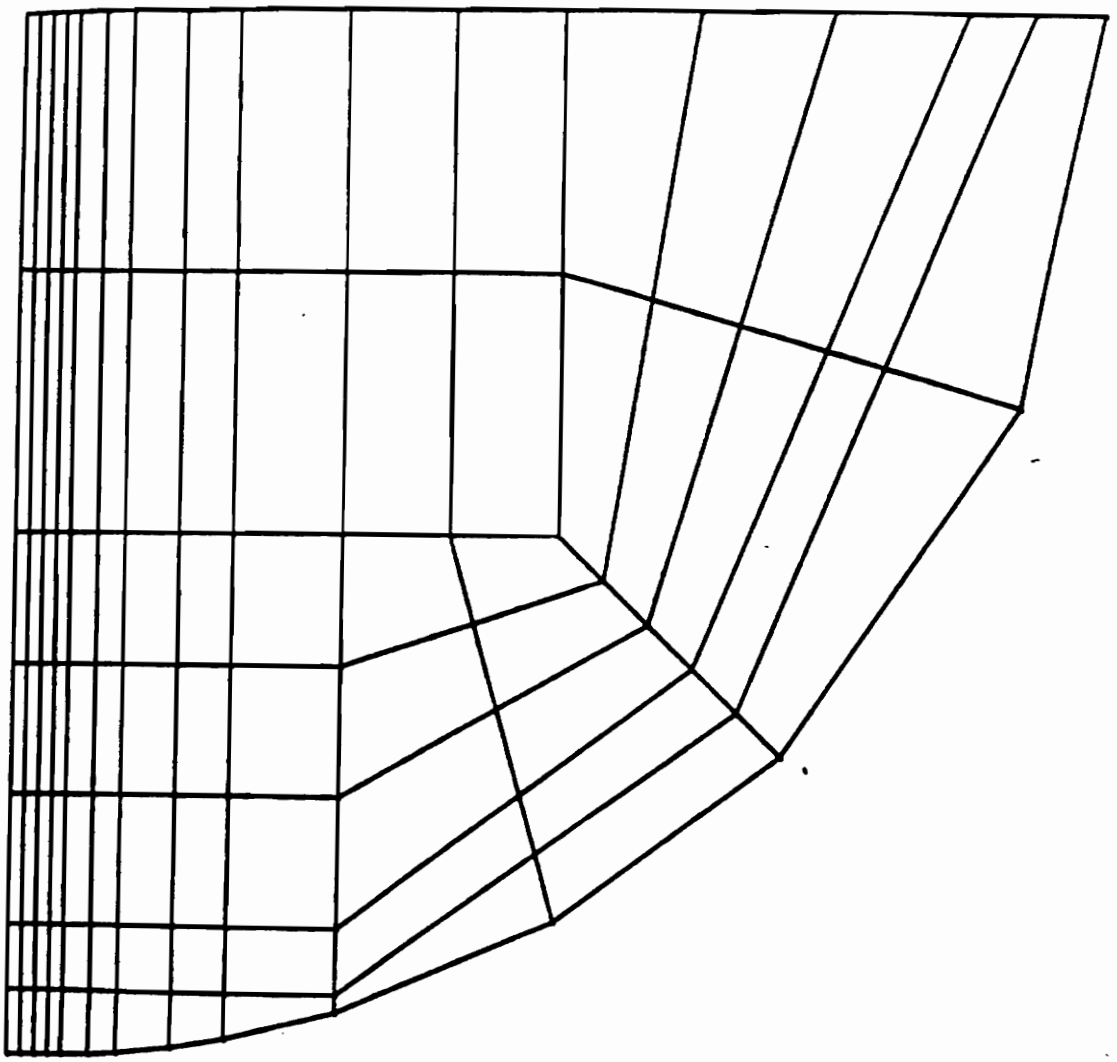

Figure 4.6. Refined finite element mesh for the Hertz contact problem

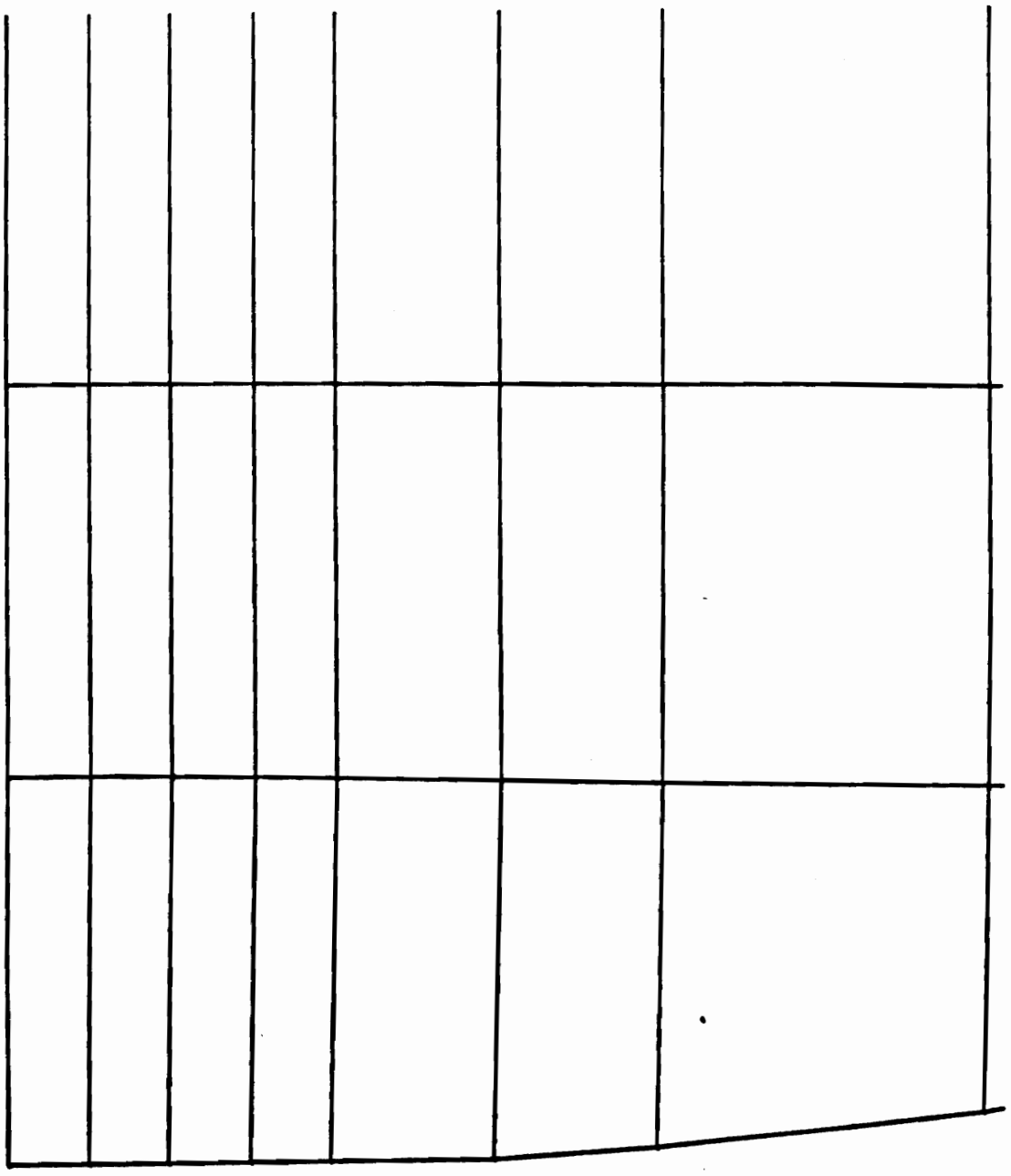

Figure 4.7. Deformed configuration (6 nodes in contact) for refined mesh

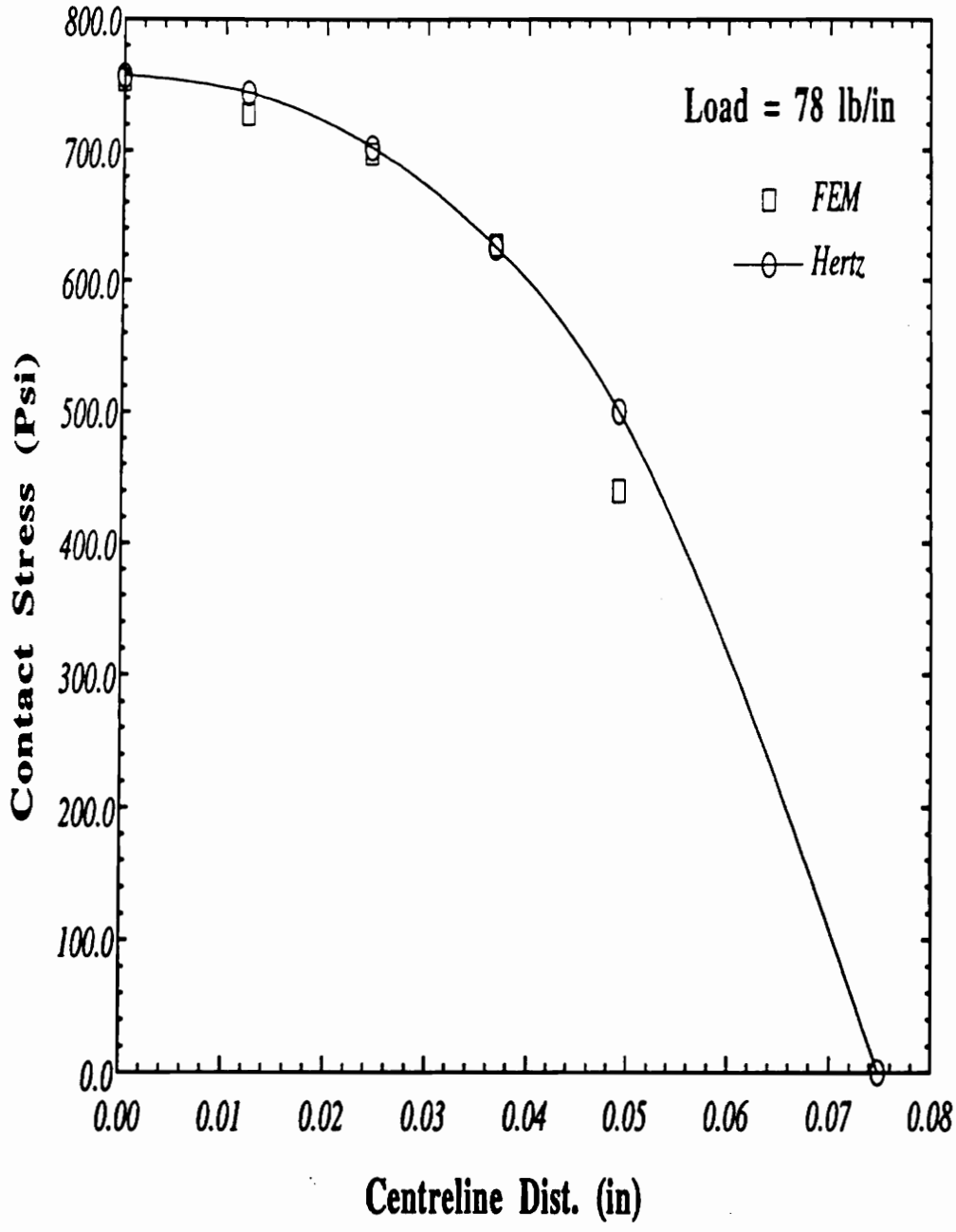

Figure 4.8. Contact pressure vs centreline distance for a load of 78 lb/in

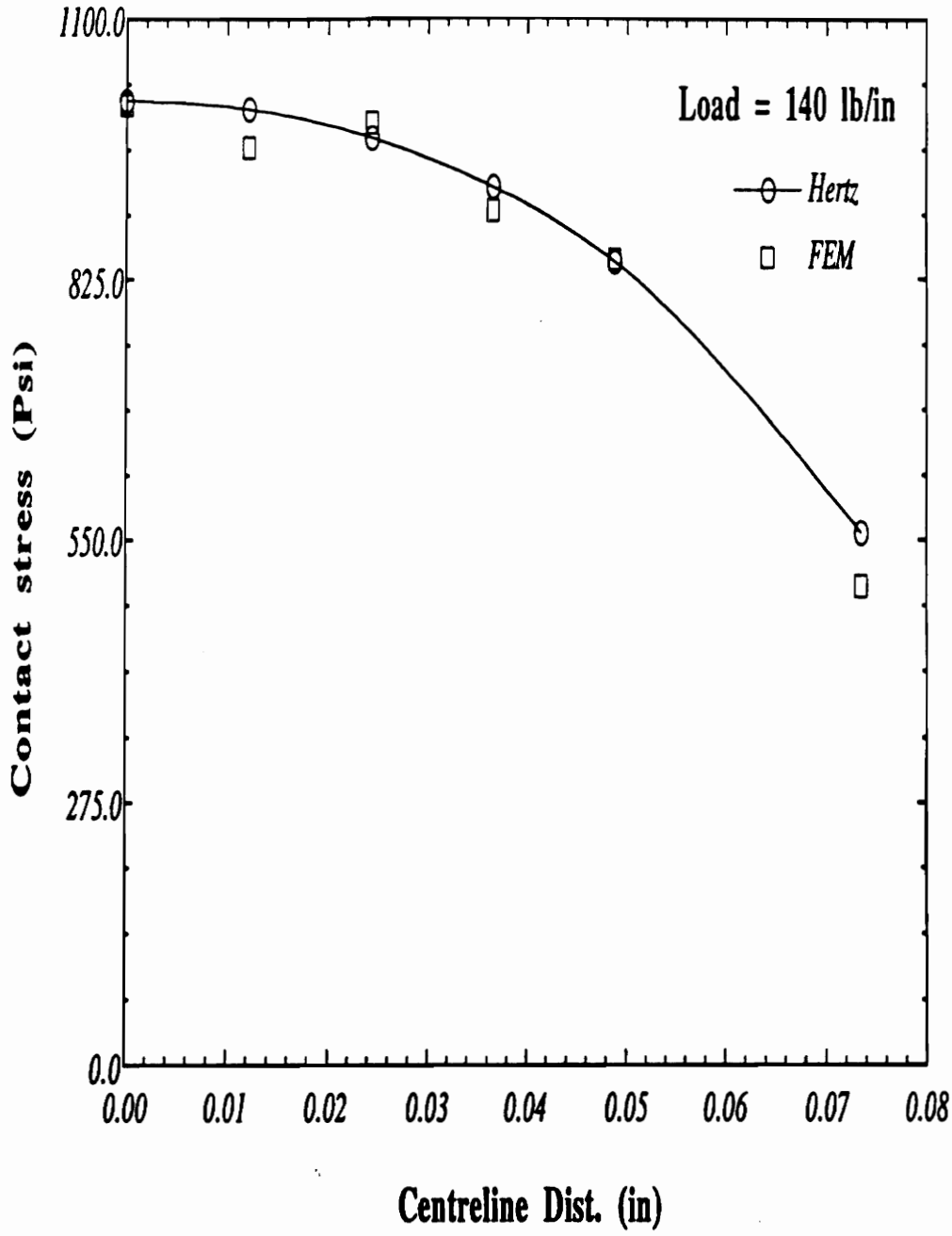

Figure 4.9. Contact pressure vs centreline distance for a load of 140 lb/in

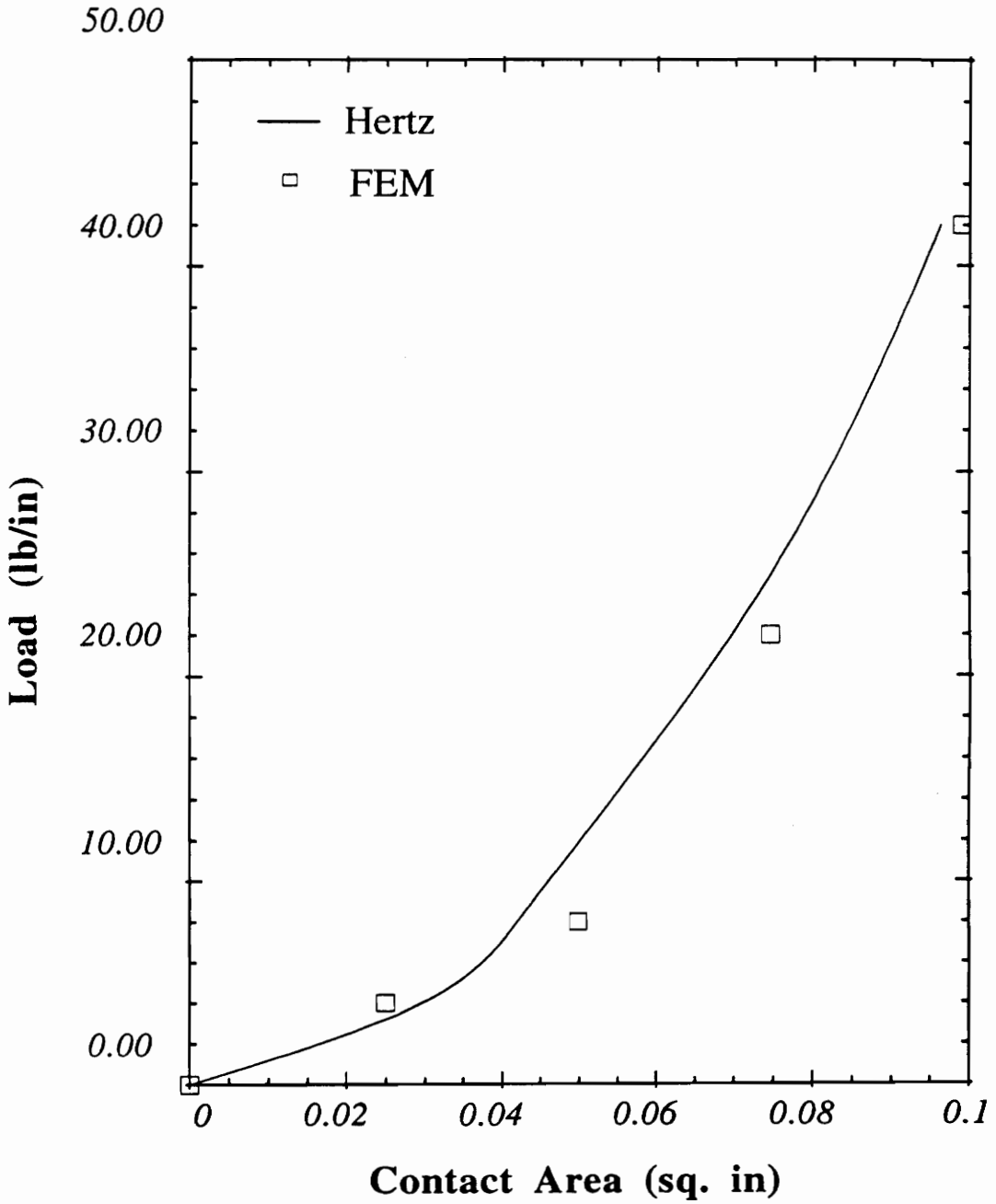

Figure 4.10. Load vs contact area for the Hertz contact problem

the centreline. It corresponds to a total applied load of 118 Psi. At this load three nodes on the boundary come into contact. Fig.[4.5] shows the contact pressure variation with centreline distance for a load of 248 lb/in. It can be seen that four nodes are in contact for this load.

The second mesh Fig.[4.6] is much finer and uses 88 isoparametric linear elements and has 530 degrees of freedom. At the maximum load of 140 lb/in, six nodes come into contact. The corresponding deformed mesh (magnified) is shown in Fig.[4.7]. Figs.[4.8] and [4.9] show the show the pressure distribution for the refined mesh. Fig.[4.10] shows the load plotted against the total contact area for the refined mesh. Since the continuous contact problem is discretized into a finite number of nodal points, the contact area variation as a function of loading is also discrete in nature. As has been mentioned in Chapter 1, this is the characteristic nonlinearity arising in a contact problem. What this means in terms of the finite element solution procedure is that the data points for the contact length can only be obtained when each successive node comes into contact with the target surface (in our case, the rigid plane). The finite element solution appears to follow quite closely the analytical solution, both for the pressure distribution and the contact area variation.

For the above analyses, the load was applied incrementally, with the initial load steps in smaller increments as compared to the later ones. A tolerance of 0.001 was used for the equilibrium iterations.

4.2 Isotropic Cylinder with a bore

As a preliminary to the layered cylinder problem, the contact algorithm was applied to the isotropic cylinder with a bore. The motivation for doing this was to verify the formulation in cylindrical coordinates against the equivalent formulation in cartesian coordinates. The Youngs modulus and Poissons ratio are the same as that used for the Hertz contact problem

i.e. 21000 Psi and 0.3 respectively. The dimensions of the cylinder modeled are an outer radius of 1.6875 inches and a bore radius of 0.75 inches. Since the line load applied at the top of the cylinder and the support are symmetrical, only half of the cylinder is modeled. The target surface in this case is also the rigid plane surface. Nine hundred linear isoparametric elements are used and the total number of degrees of freedom are 4880. The number of of degrees of freedom per node are five. Fig.[4.11] shows the finite element mesh used and the type of line load applied at at the top of the cylinder. Fig.[4.12] shows the final deformed mesh for a load of 34 lb/in. The contact pressure variation as a function of the angle about the centre of the cylinder is plotted in Fig.[4.13] and Fig.[4.14]. Three nodes are in contact when the total load is 9 lb/in and four nodes come into contact for a load of 34 lb/in. The variation of contact area in with load is given in Fig.[4.15].

The results obtained from the formulation in cylindrical coordinates were compared with those obtained using the formulation in cartesian coordinates for the case of the isotropic cylinder with a bore. They were found to be exact to four decimal places for most of the degrees of freedom. Any variation whenever it occured was minor and can be attributed to numerical computation. This close correlation lends confidence to the correctness of the formulation in cylindrical coordinates and it is applied next to the layered cylinder with a bore.

4.3 Layered cylinder with a bore

The layered cylinder with different material properties for the case and the propellant was modelled using 1200 linear isoparametric elements. The dimensions of the cylinder are the same as that of the problem in section 4.2, i.e. an outer radius of 1.6875 inches and bore radius of 0.75 inches. The thickness of the case is 0.0625 inches. A single layer of elements is used to model the case and fourteen elements for the much thicker layer of propellant in the radial direction. As discussed in Chapter 2, since the material properties of the case are different

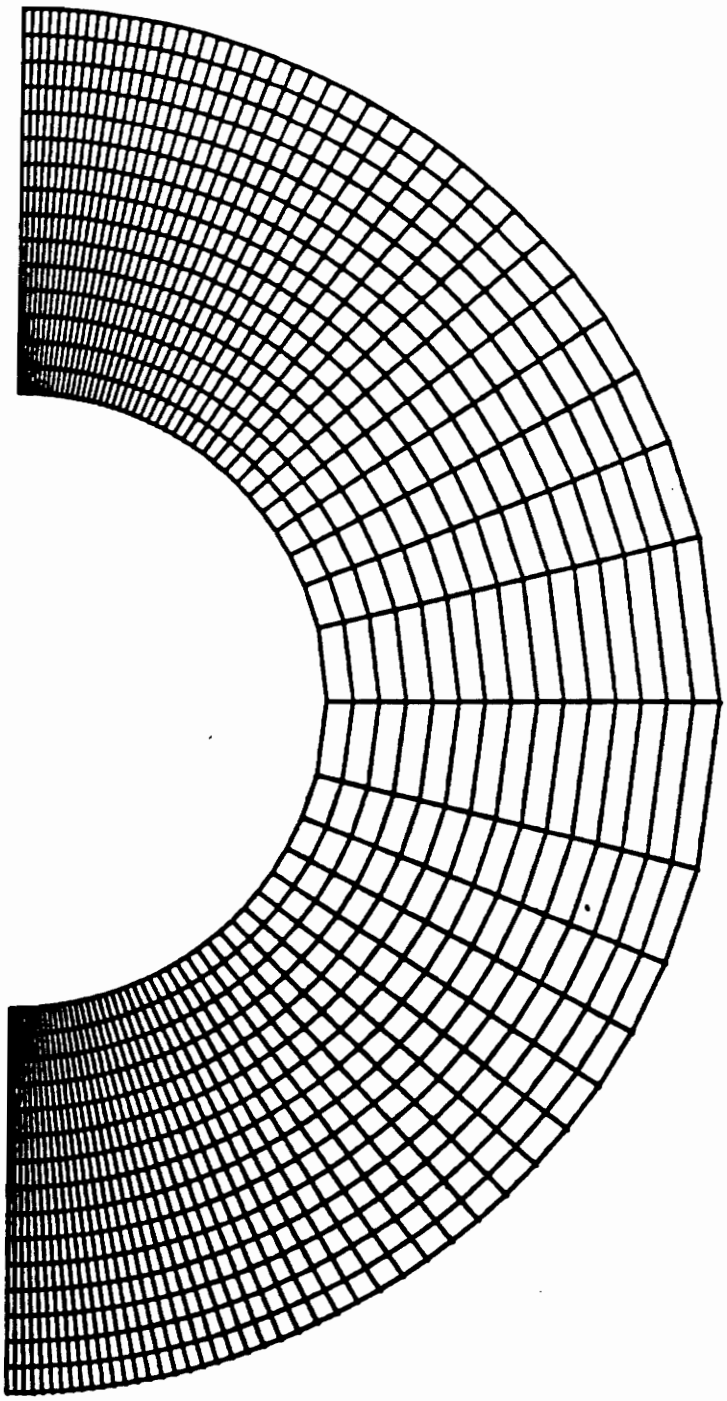

Figure 4.11. Finite element mesh for isotropic cylinder with bore

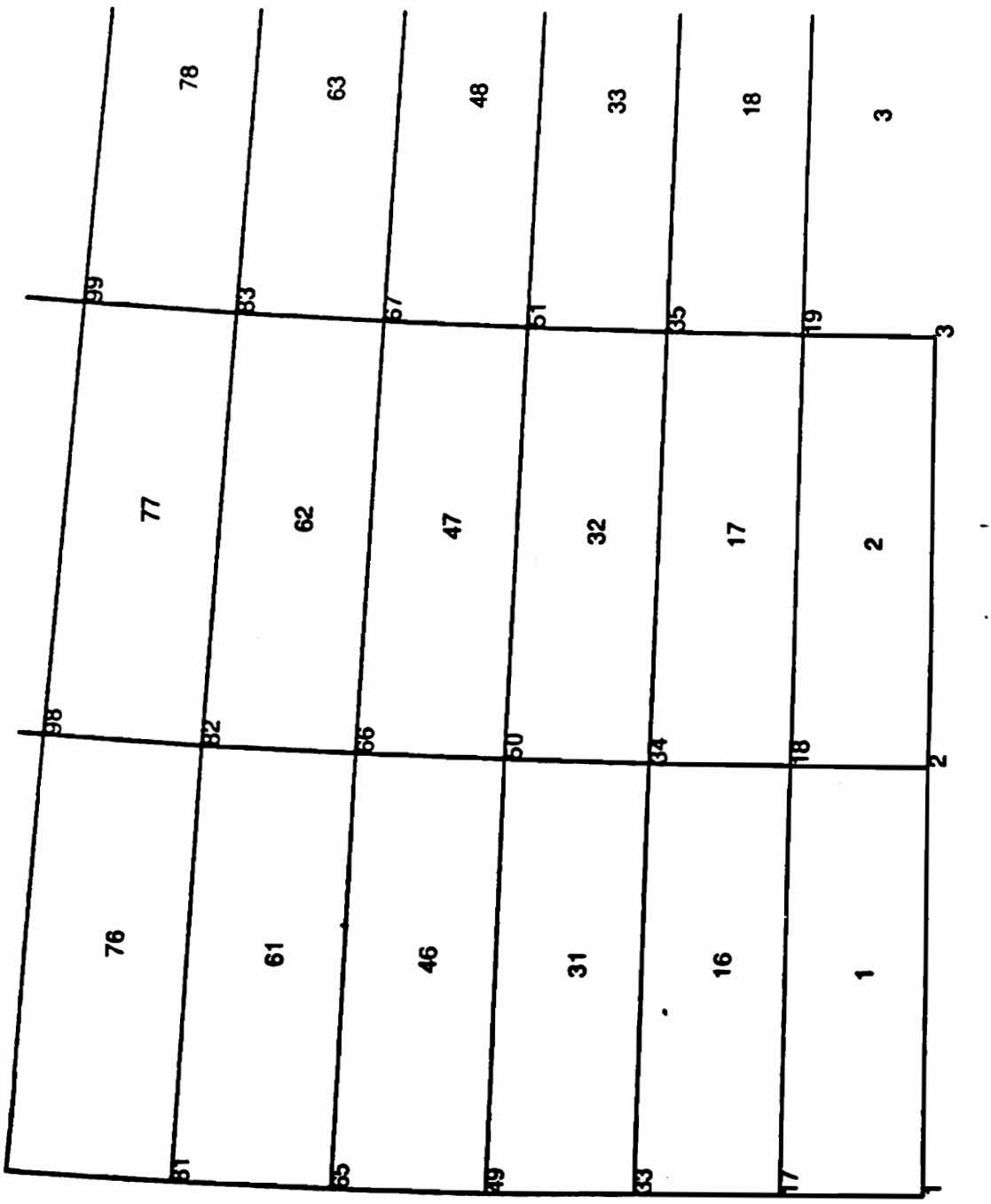

Figure 4.12. Deformed finite element mesh (nodes 1,17,33 & 49 in contact)

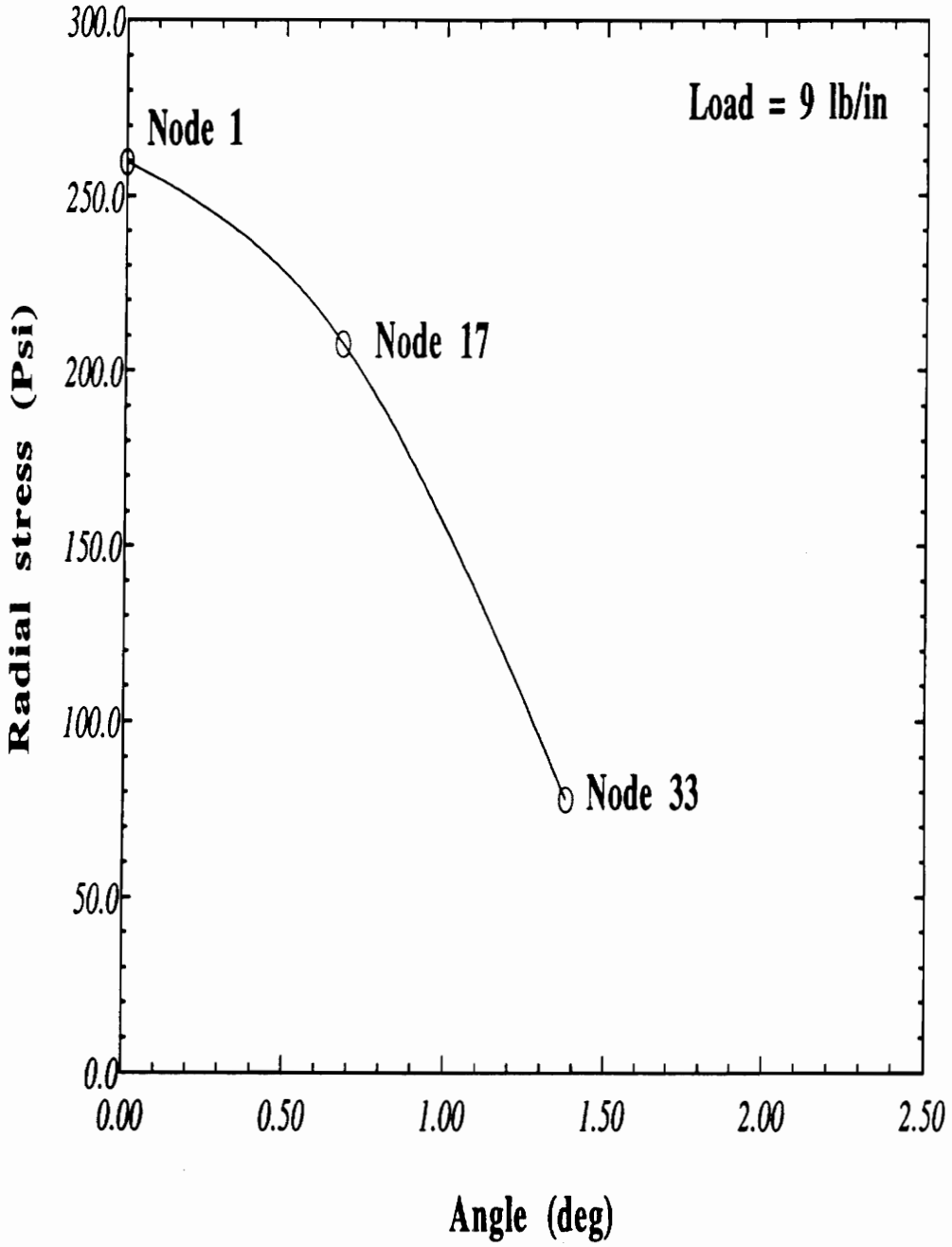

Figure 4.13. Contact stress vs angle about centre for a load of 9 lb/in

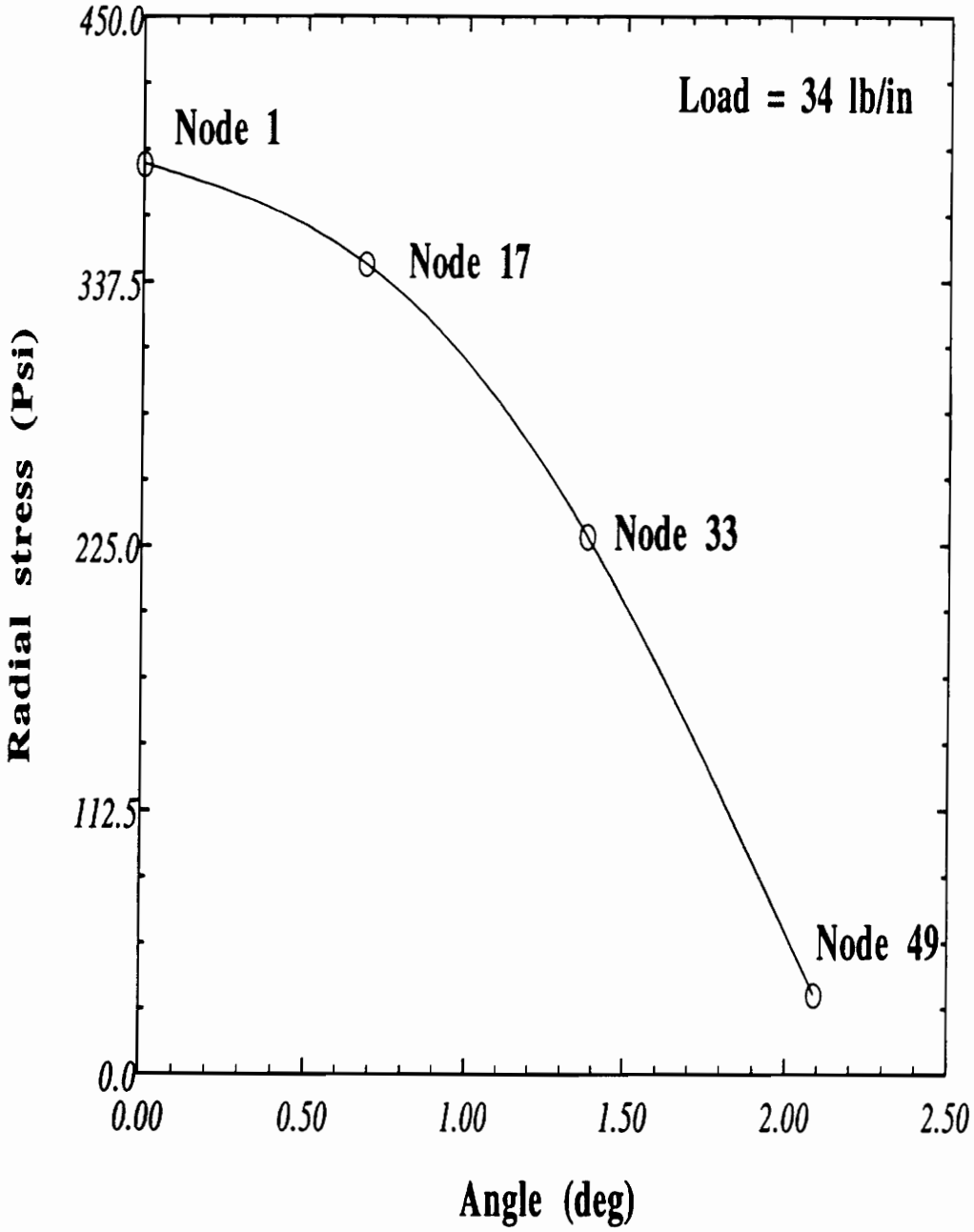

Figure 4.14. Contact stress vs angle about centre for a load of 34 lb/in

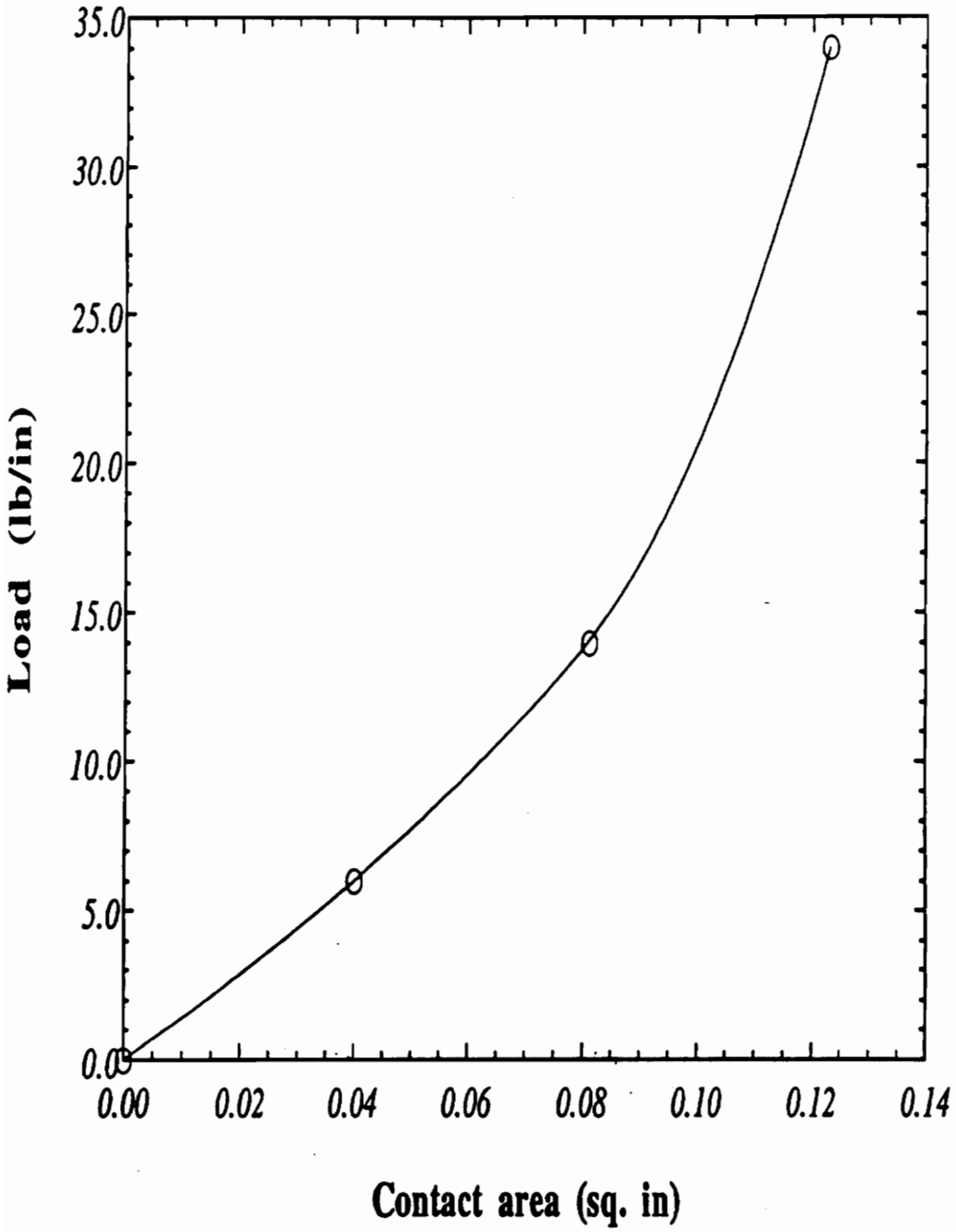

Figure 4.15. Load vs contact area for the isotropic cylinder with bore

from those of the propellant the static condensation procedure needs to be adopted to condense out the discontinuous tangential stress component. This procedure reduces the degrees of freedom per node to four from five. Hence the total degrees of freedom for this problem are 5184. The load is applied as a line load at the top of the cylinder in increments.

The Youngs modulus for the case is taken as 2.E05 Psi and the Poissons ratio is 0.3. the Youngs modulus for the propellant is 1.E04 Psi and the Poissons ratio is 0.49. The results of the contact analysis are shown in Figs.[4.16-4.20].

The nonlinear variation of the contact area with load is seen in Fig.[4.17]. The contact stress is plotted for a maximum load of 170 lb/in. At this load, four nodes are in contact Fig.[4.16]. It can be seen from the figure that the contact stress variation with distance from the centerline shows a great variation from the Hertzian distribution. The contact stress seems to decrease almost linearly as we move away from the centre as opposed to the elliptical distribution observed in the Hertzian case.

The tangential stresses in the bore Fig.[4.18] also exhibit a linear variation with load. This is to be expected since the nodes on the bore are far away from the point of application of the load. The tangential stresses at the interface between the casing and the propellant are shown in Fig.[4.19]. These results correspond to the stress obtained from the casing (since the tangential stresses are being condensed out at the element level, there will be two values of the tangential stress at a common node on the interface, one from the element that belongs to the casing and another from the element that belongs to the propellant layer). Fig.[4.19] shows that the tangential stress exhibits a steep increase with load initially. After about 100 lb/in, the gradient becomes less steep and almost levels off. Fig.[4.20] shows the tangential stress at the same node but computed from the element that belongs to the propellant layer. The stresses in this case are compressive and indicate a steady increase with load.

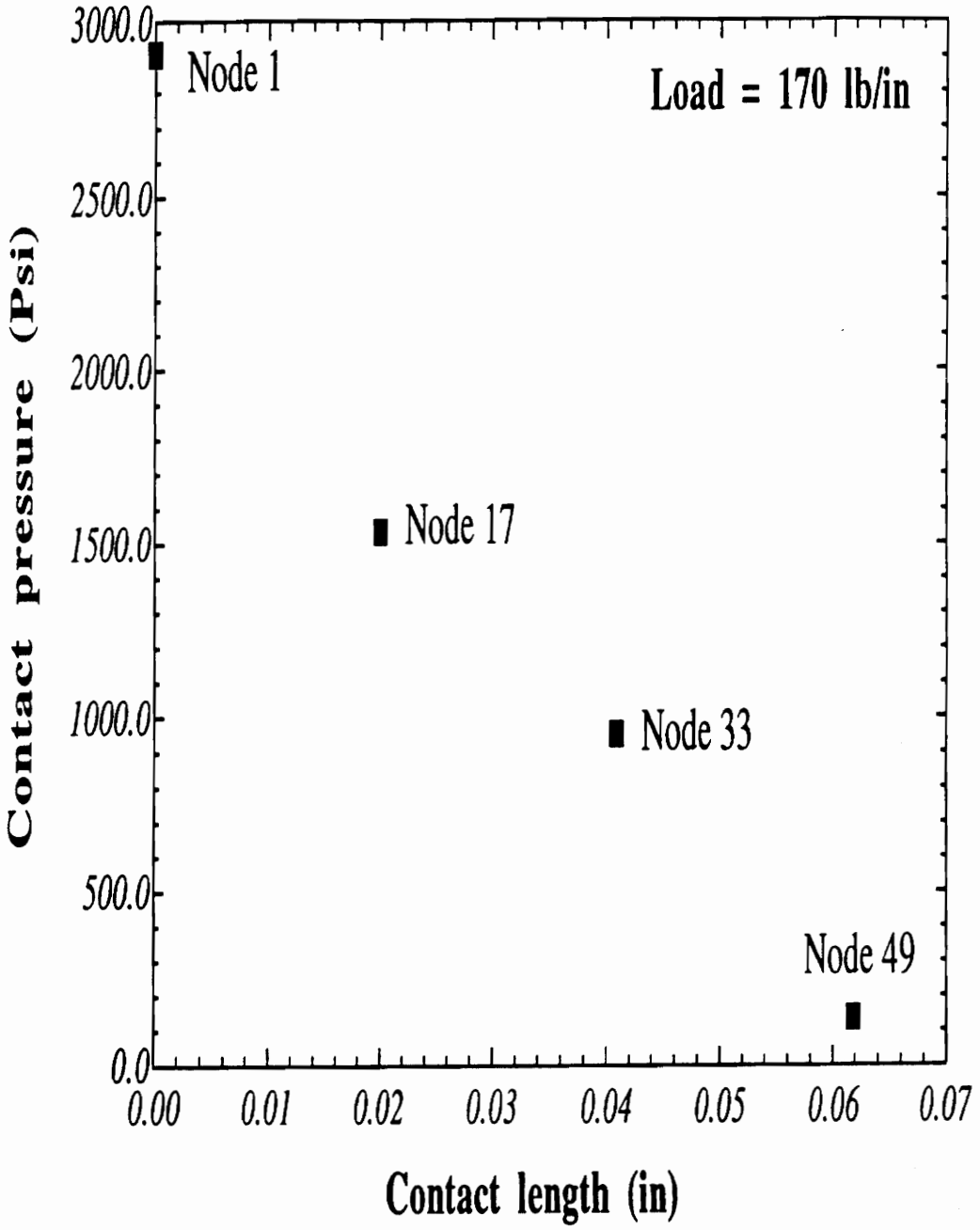

Figure 4.16. Contact stress vs centreline distance for the layered cylinder

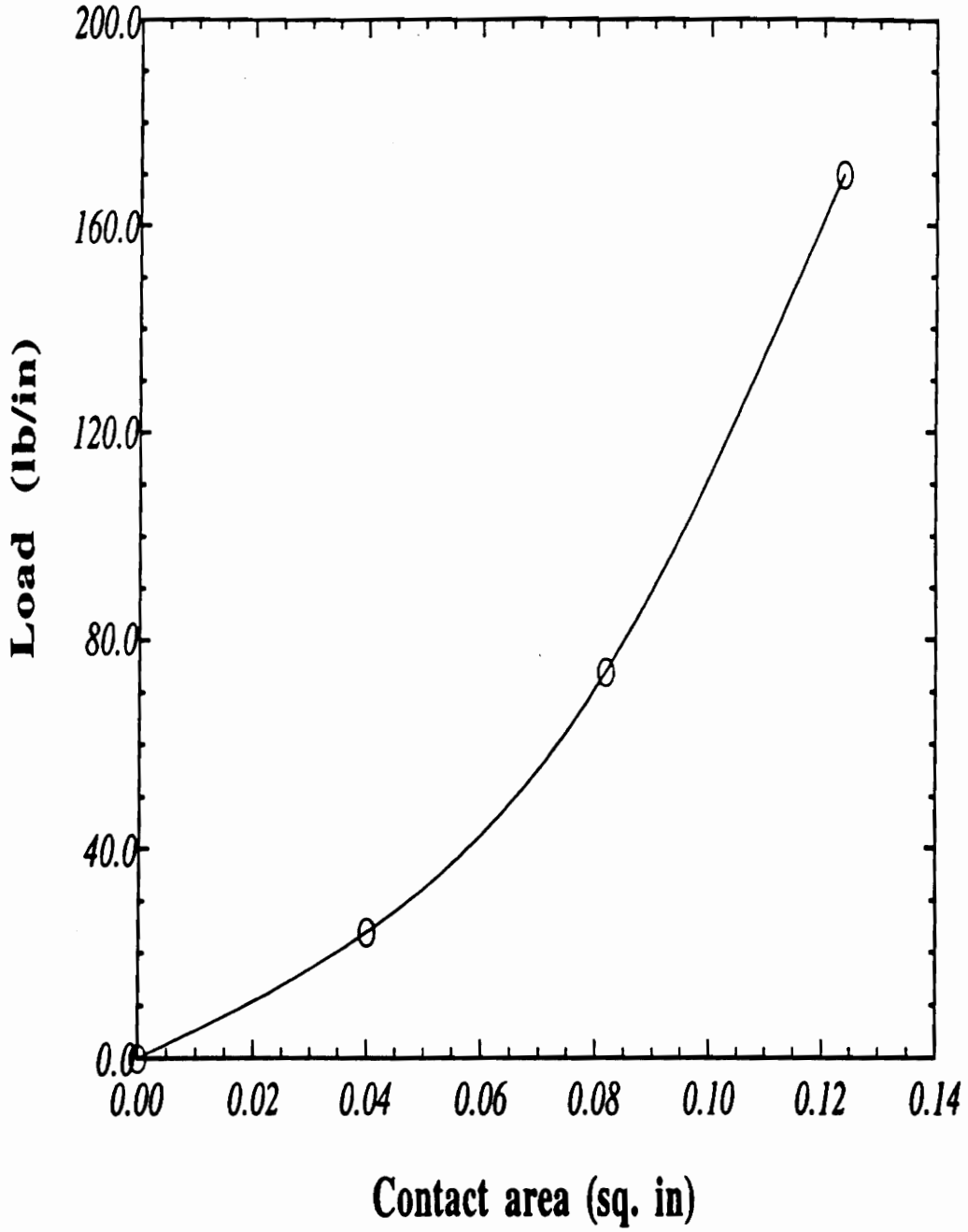

Figure 4.17. Load vs contact area for the layered cylinder

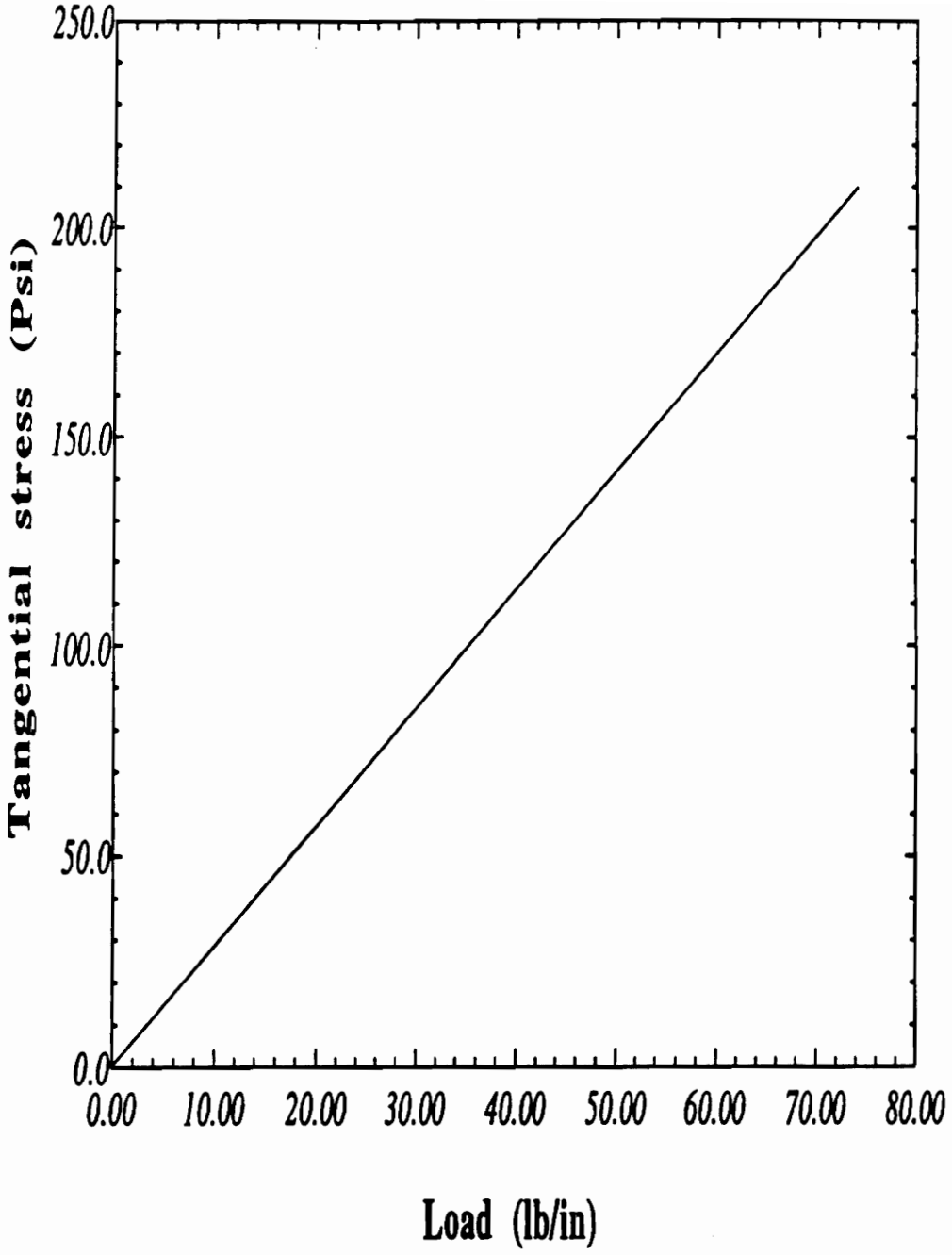

Figure 4.18. Tangential stress vs load at the bore (node 16)

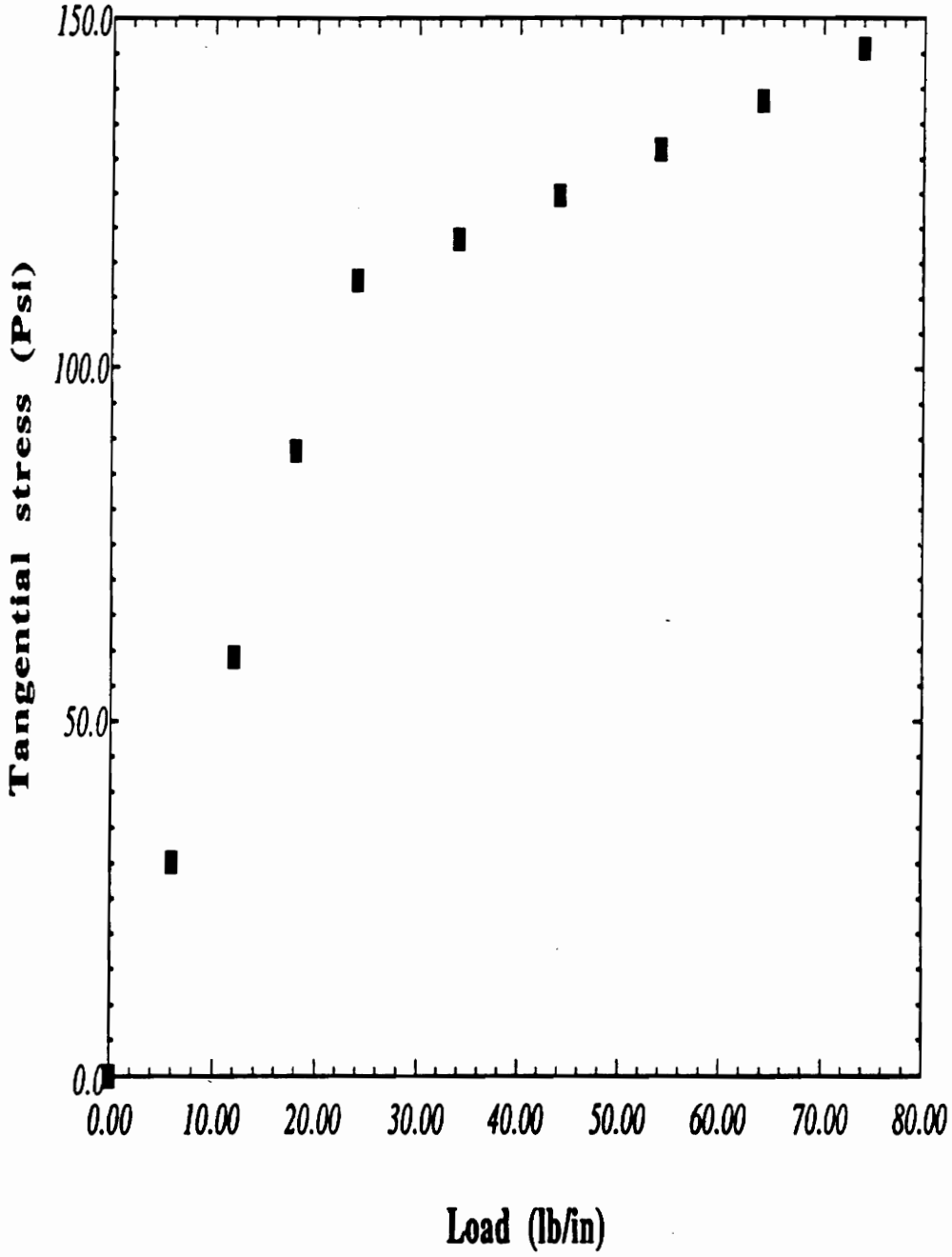

Figure 4.19. Tangential stress vs load at the interface (node 2, casing)

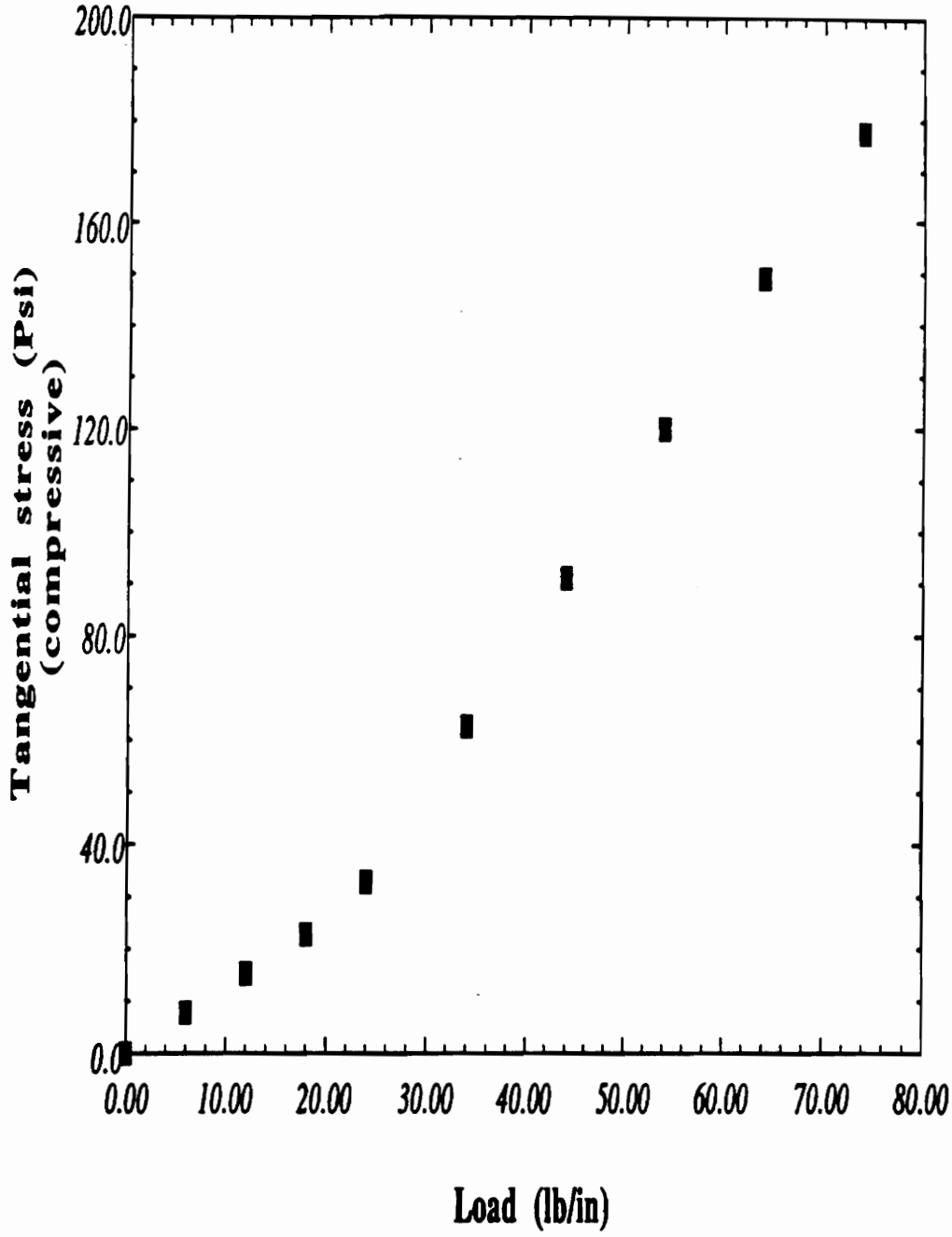

Figure 4.20. Tangential stress vs load at the interface (node 2, propellant)

Chapter V

SUMMARY, CONCLUSIONS AND RECOMMENDATIONS

5.1 Summary

A mixed formulation based on the Hellinger-Reissner variational principle is developed in cylindrical coordinates to analyse orthotropic, layered cylinders. In the mixed formulation, both displacements and stresses are approximated independently. Since the stresses are approximated independently, they are available directly from the solution vector and need not be postcomputed. Besides, in contact problems, stresses are required at the boundary nodes and the mixed formulation facilitates that purpose. It also helps to improve the accuracy of the solution since the extrapolation of the stresses computed at the Gauss points to the boundary is avoided. Another advantage of the mixed method is that it allows the specification of stress boundary conditions.

A computational algorithm based on the penalty technique for equality constraints was developed to handle the interface conditions. The effect of friction was neglected. The algorithm is capable of handling contact between a rigid surface and a deformable body. Several numerical examples for which classical solutions exist were solved to validate the algorithm.

The algorithm was also used to solve the contact problem in a layered cylinder with different material properties for each layer. The material discontinuity necessitated the use of static condensation techniques to condense out the discontinuous components of stress at the element level.

5.2 Conclusions

The results obtained by combining the mixed finite element method and a penalty technique were in good agreement with analytical solutions. The availability of stress as a nodal solution was very useful in computing the nonlinear stiffness and force matrices. Although the mixed finite element method suffers from the disadvantage that it increases the nodal degrees of freedom and thus the size of the problem to be solved, the gain in accuracy and computational ease makes up for any extra computational time spent.

The contact algorithm was found to be quite efficient in that convergence was obtained in most cases in two or three iterations. The value of the penalty parameter was selected by numerically experimenting with different values. Although, initially increasing the magnitude of the penalty parameter helped improve the imposition of the impenetrability condition, indefinitely increasing it had no appreciable effect either on the convergence or the contact conditions.

During the analysis of layered cylinders it was found that a modulus difference of more than an order of magnitude caused unpredictable bending of the cylinder and subsequent breakdown of the algorithm which depends on the systematic contact of the nodes on the boundary.

An analysis of the limiting case of a soft interior was attempted by modelling only the casing. It was found that at a particular load level, the entire shell buckled with subsequent breakdown of the contact algorithm and loss of convergence. This leads to the conclusion that when there is a soft interior the structure may buckle inwards and instead of progressive contact from the inside out, the reverse might occur. Modelling this would require incorporating some form of release conditions for the nodes on the boundary in the contact algorithm.

5.3 Recommendations

The unpredictable bending of the cylinder warrants further investigation to explore ways of modifying the algorithm to handle the contact problem for larger differences in moduli. Several other extensions to this work are possible. Friction at the contact interface can be incorporated so that different stick-slip conditions can be handled. Another relevant possibility is extending the algorithm to handle thermoelastic contact. Thermoelastic deformations arising due to a temperature difference between the contacting bodies or due to heat of friction may alter the contact geometry and thus the contact area. The algorithm could also be used as a compact subroutine in a an impact solution procedure. The contact subroutine could be called to compute the contact forces and contact area in every time step.

References

1. Kikuchi,N. and Oden,J.T. *Contact problems in elasticity: A study of variational inequalities and finite element methods*, Studies in Applied Mathematics, SIAM, Philadelphia, 1988

2. Hertz,H., "On the contact on elastic solids", *J.Math.*, V.92, pp 156-171, 1881

3. Muskhelishvili,N.I., *Some Basic Problems of the Mathematical Theory of Elasticity*, 3rd Edn., Moscow, 1949

4. Gladwell,G.M.L., *Contact problems in classical theory of elasticity*, Germantown, MD, 1980

5. Johnson,K.L., *Contact Mechanics*, Cambridge University Press, Cambridge, 1987

6. Knight,C.E., *The finite element method in mechanical design*, PWS-Kent Pub. Co., Boston, MA, 1993

7. Stadter,J.T. and Weiss,R.O., "Analysis of contact through finite element gaps", *Computers & Structures*, V.10, pp 867-873, 1979

8. Zienkiewicz,O.C., *The finite element method in engineering science*, McGraw-Hill, London, 1971

9. Reddy,J.N., *An introduction to finite element method*, McGraw-Hill, New York, 1985

10. Wilson, E.A. and Parsons,B., "Finite element analysis of elastic contact problems using differential displacements", *Int. J. Num. Meth. Engng.*, V.2, pp.387-395, 1970

11. Chan,S.K. and Tuba,I.S., "A finite element method for contact problems of solid bodies, Part I and Part II" *Int. J. Mech. Sci.*, pp.317-327, 1971

12. Ohte,S., "Finite element analysis of contact problems", *Bull. JSME*, V.16, pp.797-804, 1973

13. Tsuta,T.,and Yamaji,S., "Finite element analysis of contact problems", *Theory and practice in finite element structural analysis*, Univ. of Tokyo Press, Tokyo, pp.177-194, 1973

14. Francavilla,A. and Zienkiewicz,O.C., "A note on numerical computation of elastic contact problems", *Int. J. Num. Meth. Engng.* , V.9, pp.913-924, 1975

15. Gaertner,R., "Investigation of plane elastic conatct allowing for friction", *Computers & Structures*, V.7, pp.59-63, 1975

16. Kalker,J.J., "Variational principles of contact elastostatics", *J. Inst. math. Appl*, V.20, pp.199-219, 1977

17. Campos,L.T., Kikuchi,N. and Oden,J.T., "A numerical analysis of a class of contact problems with friction in electrostatics", *Comp. meth. in Appl. Engng.*, V.34, pp 821-845, 1982

18. Okamoto,N. and Nakazawa,M. "Finite element incremental contact analysis with various frictional conditions", *Int. J. Num. Meth. Engng*, V.14, pp.337-357, 1979

19. Sachdeva,T.D. and Ramakrishnan,C.V., "A finite element solution for the two dimensional elastic contact problems with friction", *Int. J. Num. Meth. Engng.*, V.17, pp.1257-1271, 1981

20. Oden,J.T. and Pires,E.B., "Analysis of contact problems with friction under oscillating loads", *Computer Methods in Applied Mechanics and Engineering*, V.53, pp.163-182, 1985

21. Rahman,M.U., Rowlands,R.E., Cook,R.D. and Wilkinson,D.L., "An iterative procedure for finite element stress analysis of frictional contact problems", *Computers & Structures*, V.18, N.6, pp 947-954, 1984

22. Chandrashekaran, N., Haisler,W.E. and Goforth,R.E., "Finite Element Analysis of Hertz contact problem with friction", *Finite Element Analysis and Design*, V.3, pp.39-56, 1987

23. Bathe,K.J. and Chaudhary,A., "A solution method for planar and axisymmetric contact problems", *Int. J. Num. Meth. in Engng.*, V.21, pp 65-68, 1985

24. Tseng and Olsson,M.D., "The mixed finite element method applied to two dimensional elastic- contact problems", *Int. J. Num. Meth. Engng*, V.17, pp.991-1014, 1981

25. Haslinger,J.,and Hlavacek,I., "Approximations of the Signorini Problem with friction by a mixed finite element method", *J.Math.Anal.Appl.*, V.86, pp.99-122, 1982

26. Heyliger,P.R. and Reddy,J.N., "A mixed updated Lagrangian formulation for plane elastic problems", *Journal of composites technology and research*, V.9, N.4,1987

27. Bathe,K.J., *Finite element procedures in engineering analysis*, Prentice-Hall, Englewood Cliffs, N.J., 1982

28. Mirza,F.A., "A solution technique for indefinite systems of mixed finite elements", *Int. J. Num. Meth. in Engng.*, V.20, pp 1551-1561, 1981

29. Yogeswaran,E.K. and Reddy,J.N., "A study of contact stresses in pin-loaded orthotropic plates", *Computers & Structures*, V.30, N.5, pp 1067-1077, 1988

30. Mirza,F.A. and Olson,M.D., "The mixed finite element method in plane elasticity", *Int.J.Numerical methods in Engng.*, V.15, pp 273-289, 1980

31. Heyliger,P.R., "A mixed computational algorithm based on the updated lagrangian description for plane elastic problems", *Phd. Dissertation, VPI&SU, 1986*

Vita

The author was born on May 2nd, 1969 at Madras, India. After undergoing schooling in various parts of India he obtained an undergraduate degree in Mechanical Engineering from Osmania University, Hyderabad, India, in July 1990. The same year he left for the USA in order to pursue a Masters degree in Engineering Mechanics at VPI&SU. The author obtained his Masters degree in August 1993 and plans to take up a position in industry in the general area of numerical modelling.